

# Phenomenology of the Dark Matter sector in the 2HDM extended with Complex Scalar Singlet

Juhi Dutta\*

*II. Institut für Theoretische Physik  
Universität Hamburg, Luruper Chaussee 149, 22761 Hamburg*

Gudrid Moortgat-Pick†

*II. Institut für Theoretische Physik  
Universität Hamburg, Luruper Chaussee 149,  
22761 Hamburg, Deutsches Elektronen-Synchrotron DESY,  
Notkestr. 85, 22607 Hamburg, Germany*

Merle Schreiber‡

*II. Institut für Theoretische Physik  
Universität Hamburg, Luruper Chaussee 149, 22761 Hamburg,  
Deutsches Elektronen-Synchrotron DESY,  
Notkestr. 85, 22607 Hamburg, Germany*

The Two Higgs Doublet model augmented with a complex scalar singlet (2HDMS) is a well-motivated candidate for Beyond Standard Model (BSM) Physics. We investigate the dark matter phenomenology of the 2HDMS with the complex scalar singlet as the dark matter candidate. We perform a study of the parameter space allowed by existing experimental constraints from dark matter, flavour physics and collider searches. The distinction between real and complex scalar dark matter in the context of the 2HDMS is also performed. Furthermore, we discuss the discovery potential for the 2HDMS at the HL-LHC and at future high-energy  $e^+e^-$  colliders.

## I. INTRODUCTION

Dark Matter (DM) remains a puzzle at the interface between particle physics and cosmology. In particular the nature of dark matter has been under contemplation for several decades and particle physics models providing a possible dark matter candidate are being actively explored at both theoretical and experimental frontiers. One of the possible candidates for dark matter is a scalar singlet under the Standard Model (SM) gauge group added to the SM [1–4] with the 125 GeV SM-like Higgs boson as the portal to the dark sector. Such a minimal Higgs portal dark matter model is increasingly constrained from DM direct detection experiments **Xenon-1T** data[5]. This is a strong motivation to look for non-minimal Higgs sectors, such as the Two Higgs Doublet Model (2HDM), where the enlarged Higgs sector provides additional portals to the dark sector.

The Two Higgs Doublet model (2HDM)(see Ref.[6] and references therein) is a minimal extension of the Standard Model (SM) with an extra Higgs doublet. It provides a dark matter candidate only in special cases such as the Inert Doublet model [6, 7]. Therefore, we study here an extension of the 2HDM, i.e. adding an extra singlet that provides also an natural DM candidate. While real scalar

singlet extensions of the 2HDM, have been looked into in order to address dark matter with the heavy CP-even Higgs bosons as portal to DM with discovery potential in the upcoming HL-LHC run [8–16], complex scalar extensions to the 2HDM have been studied in the context of modified Higgs sectors[17–21], pseudo-Nambu Goldstone dark matter together with a mixed Higgs sector [18, 21, 22] as well as in connection with gravitational waves signals, and in the context of axion models such as the Dine-Fischler-Srednicki-Zhitnisky (DFSZ) model [23, 24]. Scalar singlet extensions may also provide particle physics explanations for baryogenesis and gravitational waves (see [25] for the 2HDM extended with a real singlet scalar). Some of these extensions have also been studied to explain some events observed at low energy experiments such as the 95 GeV light scalar excess [15, 18, 19] as well as the neutrino anomalies[26], the (g-2) excess[27, 28] and the gamma ray excess[12, 29].

In this work, we investigate an extension of the 2HDM with a complex scalar singlet (2HDMS) in the context of dark matter, where the singlet does not develop a vacuum expectation value( $vev$ ).<sup>1</sup> This ensures that the Higgs doublet does not mix with the complex scalar resulting in the same Higgs sector as in the 2HDM, i.e. consisting of two CP-even Higgs bosons,  $h, H$ , a pseudoscalar  $A$

\* juhi.dutta@desy.de

† gudrid.moortgat-pick@desy.de

‡ merle.schreiber@desy.de

<sup>1</sup> Several interesting aspects also arise for cases where the singlet does develop a non-zero  $vev$  in 2HDMS, which we consider in an ongoing work[30].

and a pair of charged Higgs bosons  $H^\pm$ , while the complex scalar singlet serves as the DM candidate. We study the dark matter phenomenology of this model consistent with all experimental constraints including dark matter, flavour and collider constraints. The presence of the dark matter provides additional invisible decay modes for the Higgs bosons. Furthermore, associated production of the heavy Higgs bosons would lead to signatures involving visible SM quarks/leptons and missing energy signals. We choose representative benchmark points to study collider prospects at the HL-LHC and at future  $e^+e^-$  colliders and discuss the viability of observing the channel  $2b+\cancel{E}_T$  channel at an  $e^+e^-$  collider at multi TeV-range. The important points of this work include

- discussion of the parameter space allowed by dark matter constraints in 2HDMS;
- comparison between the real and complex scalar singlet models with regard to observing the differences between the dark matter phenomenology in both cases;
- identification of some representative benchmarks for 2HDMS allowed by all experimental constraints including dark matter, flavour physics and collider constraints from the SM-like Higgs boson as well as from the heavy Higgs sector;
- analysis of the collider phenomenology of the 2HDMS at the upcoming HL-LHC and at a high energy  $e^+e^-$  collider.

The paper is organized as follows: we discuss the model followed by a discussion on the relevant theoretical and experimental constraints in sec. II. Furthermore, we study two aspects: in sec. IV-V C we assume the scalar singlet does not develop a vacuum expectation value (i.e.  $v_s = 0$ ) and consider the pedagogical case where the complex scalar is the dark matter, and in sec. VI we involve the two-component formalism and apply explicitly the constraint that the singlet does not develop a vacuum expectation value. Finally, we summarise our results in Sec. VII.

## II. THE MODEL

We consider the CP-conserving Type II Two Higgs Doublet model augmented with a complex scalar singlet (2HDMS)[17] to avoid flavour changing neutral currents (FCNCs) at tree level. We consider soft  $Z_2$ -symmetry breaking consistent with tree-level FCNCs, allowing the presence of a mixing term between  $\Phi_1$  and  $\Phi_2$ , i.e.  $m_{12}^2$ . The complex scalar singlet dark matter candidate  $S$  is stabilized by a  $Z'_2$  symmetry so that  $S$  is odd under  $Z'_2$  while the SM fields are even under the new  $Z'_2$  symmetry. The quantum numbers of the fields under  $Z_2$  and  $Z'_2$  are given in Table I. The fields  $\Phi_1$  and  $S$  are even under  $Z_2$  while  $\Phi_2$  is odd under  $Z_2$ . On the other hand,

Fields	$Z_2$	$Z'_2$
$\Phi_1$	+1	+1
$\Phi_2$	-1	+1
$S$	+1	-1

TABLE I. The quantum numbers of the Higgs doublets and the singlet under the  $Z_2$  and  $Z'_2$  symmetry.

as mentioned above,  $\Phi_1$  and  $\Phi_2$  are even under the new symmetry  $Z'_2$  while  $S$  is odd under  $Z'_2$ . The  $Z'_2$  symmetry remains unbroken both explicitly as well as dynamically, i.e. the singlet does not obtain a  $vev$ . Therefore, the scalar potential  $V_{2HDMS}$  with softly broken  $Z_2$  and conserved  $Z'_2$  symmetry is

$$V_{2HDMS} = V_{2HDM} + V_S \quad (1)$$

where, the softly broken  $Z_2$ -symmetric 2HDM potential is

$$\begin{aligned} V_{2HDM} = & m_{11}^2 \Phi_1^\dagger \Phi_1 + m_{22}^2 \Phi_2^\dagger \Phi_2 - (m_{12}^2 \Phi_1^\dagger \Phi_2 + h.c.) + \\ & \frac{\lambda_1}{2} (\Phi_1^\dagger \Phi_1)^2 + \frac{\lambda_2}{2} (\Phi_2^\dagger \Phi_2)^2 + \\ & \lambda_3 (\Phi_1^\dagger \Phi_1) (\Phi_2^\dagger \Phi_2) + \lambda_4 (\Phi_1^\dagger \Phi_2) (\Phi_2^\dagger \Phi_1) + \\ & [\frac{\lambda_5}{2} (\Phi_1^\dagger \Phi_2)^2 + h.c] \end{aligned} \quad (2)$$

and the  $Z'_2$ -symmetric singlet potential,  $V_S$ , is

$$\begin{aligned} V_S = & m_S^2 S^* S + (\frac{m_S'^2}{2} S^2 + h.c.) + (\frac{\lambda_1''}{24} S^4 + h.c.) + \\ & (\frac{\lambda_2''}{6} (S^2 S^* S) + h.c.) + \frac{\lambda_3''}{4} (S^* S)^2 + S^* S [\lambda_1' \Phi_1^\dagger \Phi_1 + \\ & \lambda_2' \Phi_2^\dagger \Phi_2] + [S^2 (\lambda_4' \Phi_1^\dagger \Phi_1 + \lambda_5' \Phi_2^\dagger \Phi_2) + h.c.]. \end{aligned} \quad (3)$$

Note that the  $Z'_2$ -symmetric potential  $V_{2HDMS}$ , eq. 1, includes the U(1) symmetry breaking terms, involving  $S^2$ -,  $S^4$ -terms and the hermitian conjugates.

In terms of its components, the Higgs doublets and singlet  $S$  are parametrized as

$$\Phi_1 = (h_1^+ \quad \frac{1}{\sqrt{2}}(v_1 + h_1 + ia_1))^T, \quad (4)$$

$$\Phi_2 = (h_2^+ \quad \frac{1}{\sqrt{2}}(v_2 + h_2 + ia_2))^T, \quad (5)$$

$$S = \frac{1}{\sqrt{2}}(h_s + ia_s), \quad (6)$$

where  $v_1, v_2$  are the vacuum expectation value( $vev$ )'s obtained by the neutral components of  $\Phi_1$  and  $\Phi_2$  respectively. Since the singlet scalar does not obtain a  $vev$ , the minimization conditions are

$$m_{11}^2 = m_{12}^2 \frac{v_2}{v_1} - \lambda_1 v_1^2 - \lambda_{345} v_2^2, \quad (7)$$

$$m_{22}^2 = m_{12}^2 \frac{v_1}{v_2} - \lambda_2 v_2^2 - \lambda_{345} v_1^2, \quad (8)$$

where

$$\lambda_{345} = \lambda_3 + \lambda_4 + \lambda_5. \quad (9)$$

Particle	$h$	$H$
$u$	$\cos \alpha / \sin \beta$	$\sin \alpha / \sin \beta$
$d$	$-\sin \alpha / \sin \beta$	$\cos \alpha / \cos \beta$
$l$	$-\sin \alpha / \sin \beta$	$\cos \alpha / \cos \beta$

TABLE II. The fermion couplings in the Type II 2HDM [6].

After electroweak symmetry breaking (EWSB), there remain 15 free parameters in the model<sup>2</sup>,

$$\lambda_1, \lambda_2, \lambda_3, \lambda_4, \lambda_5, m_{12}^2, \tan \beta, \lambda_1', \lambda_3', m_S^2, m_{S'}^2, \lambda_1', \lambda_2', \lambda_3', \lambda_4'.$$

Here,  $\tan \beta = \frac{v_2}{v_1}$  is the ratio of the  $vev$ 's of the up-type and down-type Higgs doublet denoted by  $v_2 (= v \sin \beta)$  and  $v_1 (= v \cos \beta)$ , respectively, where  $v (= \frac{v_1^2 + v_2^2}{}) \simeq 246$  GeV is the electroweak  $vev$ .

### Fermion and Gauge boson sector

For the Type II 2HDM, the up and down type quarks couple to the two different Higgs doublets. The down-type quarks and leptons couple to  $\Phi_1$  while the up-type quarks couple to  $\Phi_2$ . Thus, the Yukawa Lagrangian is [6]

$$\mathcal{L}_{Yukawa} = y_u^{ij} Q_i \Phi_2 u_j - y_d^{ij} Q_i \Phi_1 d_j - y_l^{ij} L_i \Phi_1 l_j, \quad (10)$$

where  $i, j = 1, 2, 3$  are the family indices of the fermions and  $y_f$ , ( $f = u, d, l$ ) are the Yukawa coupling matrices for the quarks and leptons. The couplings of the Higgs bosons to the quarks and leptons (normalized to the SM) are summarised in Table II [6].

The Higgs bosons couple to the gauge bosons as in the 2HDM[6], namely, the  $HVV$  and  $HHVV$  couplings are suppressed by  $\cos(\beta - \alpha)$  as compared to the SM-like couplings of the Higgs boson ( $\propto \sin(\beta - \alpha)$ ). For the CP-conserving scenario, the couplings of the pseudoscalar to two gauge bosons vanish at tree level.

### Higgs sector

In the absence of mixing between the Higgs doublets and the singlet, the Higgs sector of 2HDMS remains the same as in the 2HDM after electroweak symmetry breaking, consisting of two CP-even neutral scalar Higgs bosons  $h, H$ , a pseudoscalar Higgs  $A$  and a pair of charged Higgs bosons  $H^\pm$ . The squared mass matrices for the charged ( $\mathcal{M}_\pm^2$ ), the scalar ( $\mathcal{M}_S^2$ ) and the pseudoscalar ( $\mathcal{M}_{PS}^2$ ) Higgs sectors in the gauge eigenstate

basis are given by [6],

$$M_\pm^2 = [m_{12}^2 - (\lambda_4 + \lambda_5)v_1 v_2] \begin{pmatrix} \frac{v_2}{v_1} & -1 \\ -1 & \frac{v_1}{v_2} \end{pmatrix}, \quad (11)$$

$$M_S^2 = \begin{pmatrix} m_{12}^2 \frac{v_2}{v_1} + \lambda_1 v_1^2 & -m_{12}^2 + \lambda_{345} v_1 v_2 \\ -m_{12}^2 + \lambda_{345} v_1 v_2 & m_{12}^2 \frac{v_1}{v_2} + \lambda_2 v_2^2 \end{pmatrix}, \quad (12)$$

$$M_{PS}^2 = \frac{m_A^2}{v_1^2 + v_2^2} \begin{pmatrix} v_2^2 & -v_1 v_2 \\ -v_1 v_2 & v_1^2 \end{pmatrix}, \quad (13)$$

where,

$$m_A^2 = [\frac{m_{12}^2}{v_1 v_2} - 2\lambda_5](v_1^2 + v_2^2). \quad (14)$$

After EWSB, three Goldstone bosons are eaten up by the  $W^\pm$  and  $Z$  bosons while leaving two CP-even Higgs, a pseudoscalar and a pair of charged Higgs mass eigenstates.

### Dark sector

In this work we treat the complex scalar  $S$  as the DM candidate. Driving the mass of the DM candidate  $m_\chi$  from the scalar potential at tree level, one obtains

$$m_\chi^2 = m_S^2 + \lambda_1' \frac{v_1^2}{2} + \lambda_2' \frac{v_2^2}{2}. \quad (15)$$

Note that the variables  $m_S^2$  as well as the portal couplings  $\lambda_4'$  and  $\lambda_5'$  do not contribute to the mass of the DM at tree level.

### Relevant couplings

The Higgs bosons couple to the DM candidate, giving rise to vertices  $h_i S S$ ,  $h_i h_j S S$  where  $i, j = 1, 2$ . Trilinear couplings to the pseudoscalar are absent at tree-level due to CP-conservation therefore only  $A A S S$  vertices are allowed. The trilinear couplings of the DM with the CP-even Higgs bosons, relevant for our discussion in this section, are listed below, while all other couplings are listed in the appendix.

$$\lambda_{hSS} = \frac{2v}{\sqrt{1 + \tan^2 \beta}} (\lambda_4' \sin \alpha - \lambda_5' \tan \beta \cos \alpha), \quad (16)$$

$$\lambda_{hS^*S} = \frac{v}{\sqrt{1 + \tan^2 \beta}} (\lambda_1' \sin \alpha - \lambda_2' \tan \beta \cos \alpha), \quad (17)$$

$$\lambda_{hS^*S^*} = \frac{2v}{\sqrt{1 + \tan^2 \beta}} (\lambda_4' \sin \alpha - \lambda_5' \tan \beta \cos \alpha), \quad (18)$$

<sup>2</sup> For simplicity, we set  $\lambda_1' = \lambda_2'$  without loss of generality throughout our study. This simplifying assumption was required to disentangle RGEs when implementing this model in SARAH

$$\lambda_{HSS} = \frac{-2v}{\sqrt{1+\tan^2\beta}}(\lambda'_4 \cos\alpha + \lambda'_5 \tan\beta \sin\alpha), \quad (19)$$

$$\lambda_{HS^*S} = \frac{-v}{\sqrt{1+\tan^2\beta}}(\lambda'_1 \cos\alpha + \lambda'_2 \tan\beta \sin\alpha), \quad (20)$$

$$\lambda_{HS^*S^*} = \frac{-2v}{\sqrt{1+\tan^2\beta}}(\lambda'_4 \cos\alpha + \lambda'_5 \tan\beta \sin\alpha). \quad (21)$$

### Complex singlet scalar potential in terms of two real scalars

In this subsection, we discuss an alternate representation of the complex scalar singlet potential in terms of its real components  $h_s$  and  $a_s$ . After EWSB, the quadratic terms of the singlet potential are,

$$V_S^{(2)} = \frac{1}{4}h_s^2(m_S^2 + m_S'^2 + (\lambda'_1 + 2\lambda'_4)v_1^2 + (\lambda'_2 + 2\lambda'_5)v_2^2) + \frac{1}{4}a_s^2(m_S^2 - m_S'^2 + (\lambda'_1 - 2\lambda'_4)v_1^2 + (\lambda'_2 - 2\lambda'_5)v_2^2). \quad (22)$$

The squared masses of the mass eigenstates in the dark sector are

$$m_{h_s}^2 = \frac{1}{2}(m_S^2 + m_S'^2 + (\lambda'_1 + 2\lambda'_4)v_1^2 + (\lambda'_2 + 2\lambda'_5)v_2^2), \quad (23)$$

$$m_{a_s}^2 = \frac{1}{2}(m_S^2 - m_S'^2 + (\lambda'_1 - 2\lambda'_4)v_1^2 + (\lambda'_2 - 2\lambda'_5)v_2^2) \quad (24)$$

and the mass squared difference between  $h_s$  and  $a_s$  is,

$$\Delta^2 = |m_{h_s}^2 - m_{a_s}^2| = m_S'^2 + 2\lambda'_4 v_1^2 + 2\lambda'_5 v_2^2 \quad (25)$$

Note that in absence of  $m_S'^2$ ,  $\lambda'_4$  and  $\lambda'_5$ , i.e. U(1) symmetric case, both  $h_s$  and  $a_s$  are mass degenerate and represent a two-component dark matter scenario (see Ref.[1] and references therein for a similar study in SM extensions). For the  $Z'_2$  symmetric case, non-zero U(1) breaking terms lead to two non-degenerate mass eigenstates. Depending on the lifetime of the mass eigenstates, either both or only the lightest component will be the dark matter candidate.

The interaction terms in the singlet scalar potential are

$$V_{int} = \frac{1}{48}[\lambda_1''(h_s^2 - a_s^2)^2 + 3\lambda_3''(h_s^2 + a_s^2)^2 + 4\lambda_2''(h_s^4 - a_s^4)]. \quad (26)$$

The singlet components interact with the Higgs bosons via the trilinear and the quartic interaction terms at tree

level. The –for our discussion relevant–trilinear couplings are:

$$\lambda_{hh_s h_s} = -2v(\lambda'_1 + 2\lambda'_4) \cos\beta, \quad (27)$$

$$\lambda_{Hh_s h_s} = -2v(\lambda'_2 + 2\lambda'_5) \sin\beta, \quad (28)$$

$$\lambda_{ha_s a_s} = -2v(\lambda'_1 - 2\lambda'_4) \cos\beta, \quad (29)$$

$$\lambda_{Ha_s a_s} = -2v(\lambda'_2 - 2\lambda'_5) \sin\beta. \quad (30)$$

## III. CONSTRAINTS

### A. Conditions for imposing no $v_{ev}$ for the singlet

In order for the complex scalar to be the dark matter candidate, the singlet vev  $v_s$  must be 0. We minimize the scalar potential in the component form.

In order for the complex scalar to be the dark matter candidate, the singlet vev  $v_s$  must be 0. We minimize the scalar potential in the component form. The minimization conditions are

$$\frac{\partial V}{\partial h_s} = 0, \frac{\partial V}{\partial a_s} = 0 \quad (31)$$

Therefore, the conditions for imposing  $v_s = 0$  are

$$m_S^2 + m_S'^2 + (\lambda'_1 + 2\lambda'_4)v_1^2 + (\lambda'_2 + 2\lambda'_5)v_2^2 > 0 \quad (32)$$

$$m_S^2 - m_S'^2 + (\lambda'_1 - 2\lambda'_4)v_1^2 + (\lambda'_2 - 2\lambda'_5)v_2^2 > 0 \quad (33)$$

### B. Boundedness-from-below conditions

Boundedness-from-below (BFB) of the scalar potential ensures that  $V_{2HDM S} \geq 0$ . In this work, due to the multiple possible scalar directions and a vast number of terms in the potential, the computation of the BFB conditions is complicated. The results in this paper do not include the effect of the BFB conditions but for future studies, one must also impose the boundedness-from-below conditions and we do this numerically in an ongoing work [30].

### C. Experimental constraints

The following experimental constraints are imperative for any BSM model.

- The lightest CP-even Higgs mass ( $m_h$ ) is measured as  $125.25 \pm 0.17$  GeV within the experimental error[31]
- The invisible decay width of the light Higgs boson is constrained by ATLAS and CMS as given below,

$$BR(h \rightarrow \chi\chi) \leq 0.11^{+0.04}_{-0.03} \text{ (ATLAS)}[32] \quad (34)$$

$$\leq 0.19 \text{ (CMS)}[33].$$

This limit is adhered to the choice of  $m_{DM} > 62.5$  GeV.

- Flavour physics constraints, as taken into account, namely  $BR(b \rightarrow s\gamma) = (3.55 \pm 0.24 \pm 0.09) \times 10^{-4}$  [34],  $BR(B_s \rightarrow \mu^+\mu^-) = (3.2^{+1.4+0.5}_{-1.2-0.3}) \times 10^{-9}$  [35, 36]. The benchmark points also respect the upper limit of  $\Delta(g-2)_\mu = 261(63)(48) \times 10^{-11}$  [37].
- The benchmark points satisfy the electroweak precision test constraints on the STU parameters, where  $S = 0.02 \pm 0.1$ ,  $T = 0.07 \pm 0.12$ ,  $U = 0.00 \pm 0.09$  [38].
- The relic density upper limit is adhered to from PLANCK data, i.e,  $\Omega h^2 = 0.119$  [39].
- The DM-nucleon spin-independent cross sections satisfy constraints from XENON-1T [5] and the indirect detection constraints are taken from Fermi-LAT [40, 41].
- Collider constraints from LEP [42] and Run 2 ATLAS/CMS searches on the heavy Higgs searches [43, 44] and the 125 GeV Higgs signal strength measurements [45] have been taken into account.

The Higgs sector of the 2HDMS is the same as in the 2HDM (for the current status refer to [46, 47]). For the 2HDMS, we compute the DM relic and direct detection constraints using micrOMEGAS [48]. Constraints on the Higgs sector are checked using HiggsBounds and HiggsSignals [49]. Constraints from B-physics are checked using SPheno-v4.0.4 [50].

#### IV. DARK MATTER PHENOMENOLOGY

In the absence of a vacuum expectation value, the complex scalar singlet  $S$  acts as a dark matter candidate. It interacts with the SM particles via the Higgs bosons which act as scalar mediators. Therefore, no spin-dependent interactions occur for the dark matter candidate and the only stringent constraints arise from the spin-independent DM-nucleon direct detection searches. We discuss briefly the theoretical framework for the computation of the relic density and direct detection cross sections. For the numerical computation of the DM observables as shown in the later half of the study, we have used micrOmegas-v5.2.4 [48].

##### Relic density

For thermal dark matter, i.e, where the DM and SM are in thermal equilibrium, the processes contributing to relic density are the annihilation and the co-annihilation

process of the DM with the SM particles, see Fig. 1-3. Since the only interaction of the DM candidate to the SM particles is via the Higgs bosons (at tree-level), only s-channel Higgs  $h(H)$  mediated channels as shown in Fig. 2 contribute besides t-channel contributions mediated via  $S(S^*)$ , see Fig. 3. Therefore the relic density depends on the portal couplings  $\lambda'_1, \lambda'_2, \lambda'_4, \lambda'_5$  as well as the DM self-couplings  $\lambda''_1, \lambda''_3$ .

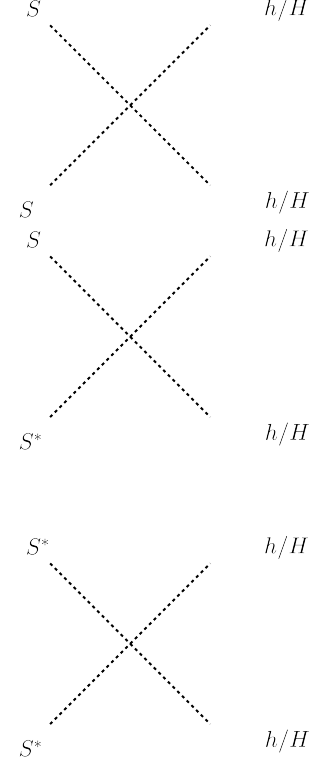


FIG. 1. The four-point vertices contribute to the computation of the relic density.

##### Spin-Independent Direct Detection cross section

The interaction of the DM with nucleon are mediated by the t-channel neutral scalar Higgs bosons at tree-level. The relevant processes are summarised in Fig. 4. The possible vertices involved in these processes are  $\lambda_{h_i SS^*}$ ,  $\lambda_{h_i SS}$  and  $\lambda_{h_i S^* S^*}$ . The latter two are DM number non-conserving while the former is DM number conserving. For a  $Z'_2$ -symmetric theory, there is apriori no reason for DM number to be conserved, since all the vertices are allowed by symmetry. Assuming a conserved DM quantum number at ultra-violet (UV) scales [51, 52], the direct detection cross sections depend solely on the coupling  $\lambda_{h_i SS^*}$  which contributes to the direct detection cross section. Note that this is solely the consequence of an underlying conserved charge corresponding to the dark matter number in presence of the discrete  $Z'_2$  symmetry. For the  $Z'_2$  symmetry breaking, the other vertices

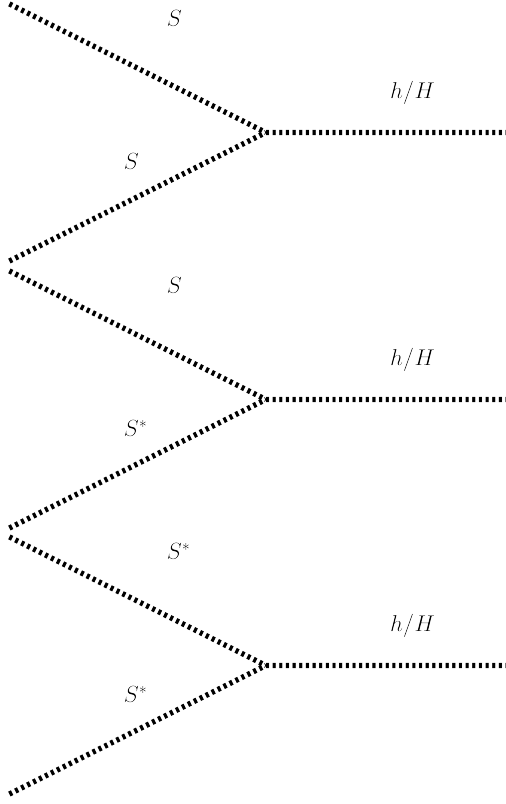


FIG. 2. The vertices contributing to the  $s$ -channel Higgs mediated processes contributing to the relic density. The Higgs bosons decay to all possible final states including fermions, gluons, gauge bosons as well as lighter Higgs bosons arising from the decay of the heavier CP-even Higgs.

$\lambda_{h_i SS}$  and  $\lambda_{h_i S^* S^*}$  may also contribute at the same order to the cross section and hence stringently constrain the current parameter space. We leave this analysis for future work and proceed with the assumption of a conserved quantum number for the DM i.e., in our study we set  $\lambda_{h_i SS}$  and  $\lambda_{h_i S^* S^*}$  to zero. The direct detection cross section rate for the proton and neutron scattering are

$$\sigma_p^{SI} = \frac{4\mu_N^2}{\pi} [f_p Z]^2, \quad (35)$$

$$\sigma_n^{SI} = \frac{4\mu_N^2}{\pi} [f_n (A - Z)]^2, \quad (36)$$

where

$$\mu_N = \frac{m_N m_\chi}{m_N + m_\chi} \quad (37)$$

is the reduced mass of the DM-nucleon system where  $N = p, n$  is the nucleon. The couplings of the proton  $f_p$  and neutron  $f_n$  and to the DM are computed from the DM-quark scattering amplitudes, see eq. 38. The heavy Higgs-mediated process would be relatively suppressed compared to the SM Higgs-mediated process due

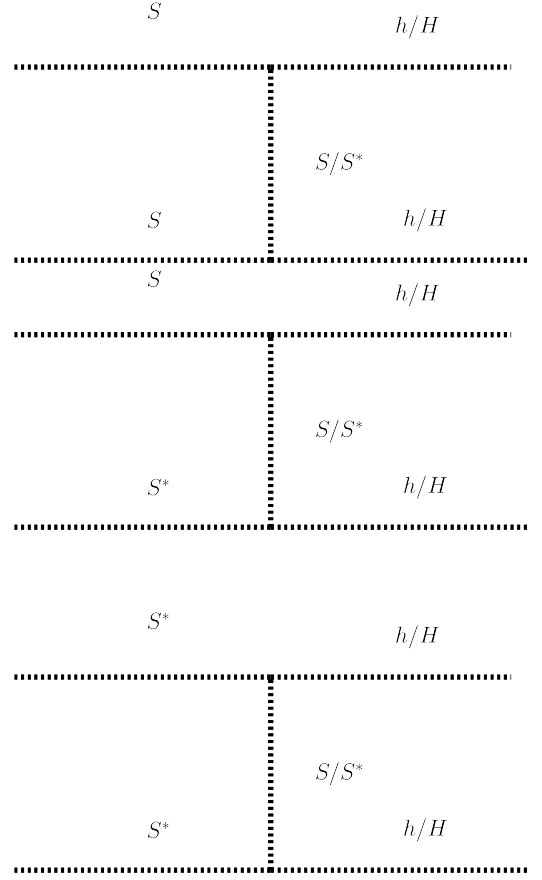


FIG. 3. The  $t$ -channel mediated processes that contribute to the relic density.

to  $m_H > m_h$ . The DM-quark amplitude  $\mathcal{M}$  is,

$$\mathcal{M} = \sum_i \frac{\lambda_{h_i SS^*} \lambda_{h_i q \bar{q}}}{t - m_{h_i}^2} \quad (38)$$

where  $i = 1, 2$  such that  $h_i = h, H$  and  $h_i q \bar{q}$  are the Yukawa couplings of the quarks to the Higgs bosons. Assuming DM number conservation and for zero momentum transfer, the propagator reduces to  $\frac{1}{-m_{h_i}^2}$ .

In the  $U(1)$  symmetric case, the two contributions to the scattering amplitudes from  $h$  and  $H$  cancel as pointed out in [53]. This is unaffected by the presence of loop-suppressed dimension-4 (and higher dimension operators)  $U(1)$  breaking terms [53, 54]. For the  $Z'_2$  symmetric case, these terms occur at the tree level (i.e.,  $S^2$ ,  $S^2 \Phi_1^\dagger \Phi_1$ ,  $S^2 \Phi_2^\dagger \Phi_2$  and their hermitian conjugates) and the direct detection cross section may be affected by the presence of the portal terms at the tree level. In this work, we do not consider the DM number violation and the only relevant contribution of the associated portal couplings to these terms (i.e.,  $\lambda'_4$  and  $\lambda'_5$ ) to the direct detection cross section arises from the  $h_i S S^*$  vertex.

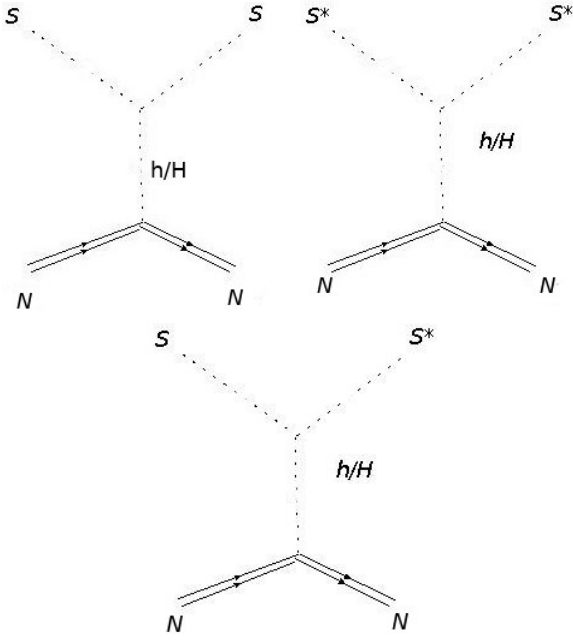


FIG. 4. Processes contributing to the direct detection of the dark matter candidate  $S$ . Here,  $N$  refers to the nucleon (proton or neutron). Assuming DM number conservation, only the right diagram involving the vertex  $hSS^*$  would contribute while the rest are DM number non-conserving.

### Indirect detection

Dark matter self-annihilation and the interactions via the CP-even Higgs bosons and their decays into final state SM particles lead to indirect detection signatures. Among these signatures, stringent constraints arise from Fermi-LAT[40, 41] on the channels  $b\bar{b}$  and  $\tau\tau$  followed by  $W^+W^-$ . For Higgs portal models the relevant annihilation channels are di-Higgs channels which are relatively weakly constrained from experiments.

## V. CASE A: COMPLEX SCALAR AS DARK MATTER

In this section, we consider the complex scalar singlet as the DM candidate assuming it does not obtain any vacuum expectation value ( $vev$ ), i.e.,  $v_s = 0$ . We discuss the relevant couplings of the dark matter in this case followed by a scan of the allowed parameter regions from the dark matter constraints of relic density and spin-independent direct detection cross section. The model is implemented using SARAH-v4.14.3[55] and SPheno-4.0.4[50] is used for generating the particle mass spectra and decays, and for performing the parameter scans. We start with a scan using the parameters summarised in Table III for obtaining a pedagogical understanding of the parameter dependencies without imposing the theoretical constraints in

this part of the study.<sup>3</sup> We consider the impact of the theoretical conditions in more detail in sec. VI.

### Relevant couplings

The scalar Higgs bosons couple to the dark matter via trilinear and quartic interactions. Trilinear couplings to the pseudoscalar Higgs are absent at the tree level due to CP-conservation therefore only  $AASS$  vertices are allowed. We list the relevant trilinear couplings of the DM with the CP-even Higgs bosons relevant for our upcoming discussions while the rest are listed in the appendix.

$$\lambda_{hSS} = \frac{2v}{\sqrt{1 + \tan^2 \beta}} (\lambda'_4 \sin \alpha - \lambda'_5 \tan \beta \cos \alpha), \quad (39)$$

$$\lambda_{hS^*S} = \frac{v}{\sqrt{1 + \tan^2 \beta}} (\lambda'_1 \sin \alpha - \lambda'_2 \tan \beta \cos \alpha), \quad (40)$$

$$\lambda_{hS^*S^*} = \frac{2v}{\sqrt{1 + \tan^2 \beta}} (\lambda'_4 \sin \alpha - \lambda'_5 \tan \beta \cos \alpha), \quad (41)$$

$$\lambda_{HSS} = \frac{-2v}{\sqrt{1 + \tan^2 \beta}} (\lambda'_4 \cos \alpha + \lambda'_5 \tan \beta \sin \alpha), \quad (42)$$

$$\lambda_{HS^*S} = \frac{-v}{\sqrt{1 + \tan^2 \beta}} (\lambda'_1 \cos \alpha + \lambda'_2 \tan \beta \sin \alpha), \quad (43)$$

$$\lambda_{HS^*S^*} = \frac{-2v}{\sqrt{1 + \tan^2 \beta}} (\lambda'_4 \cos \alpha + \lambda'_5 \tan \beta \sin \alpha). \quad (44)$$

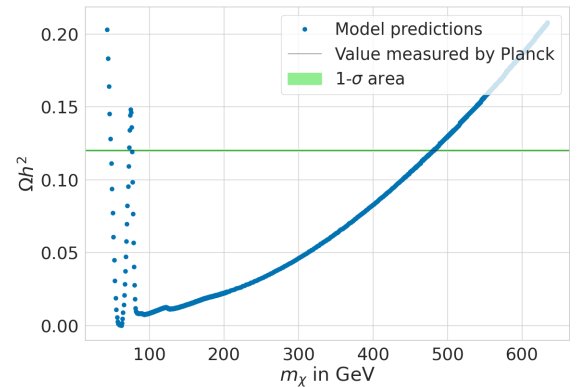


FIG. 5. The relic density predicted by the model depending on the DM mass  $m_\chi$ . The parameter  $m_S^2$  is varied in this plot in the range given in Table IV. The other input parameters are fixed as in Table III.

<sup>3</sup> Although there are constraints from the vanishing of  $vev$  on the combination of  $m_S^2$  and  $m_S^{2'}$ , we have checked that our analysis is independent of  $m_S^{2'}$ . Note that in this part of the study, we used  $m_{12}^2 \rightarrow -m_{12}^2$ .

Parameters	BPA
$\lambda_1$	0.23
$\lambda_2$	0.25
$\lambda_3$	0.39
$\lambda_4$	-0.17
$\lambda_5$	0.001
$m_{12}^2$ (GeV <sup>2</sup> )	$-1.0 \times 10^5$
$\lambda_1''$	0.1
$\lambda_3''$	0.1
$\lambda_1'$	0.042
$\lambda_2'$	0.042
$\lambda_4'$	0.1
$\lambda_5'$	0.1
$m_S^{2'}$ (GeV <sup>2</sup> )	$1.13 \times 10^5$
$m_h$ (GeV)	125.1
$m_H$ (GeV)	724.4
$m_A$ (GeV)	724.4
$m_{H^\pm}$ (GeV)	728.3
$m_\chi$ (GeV)	338.9
$\tan \beta$	5

TABLE III. List of parameters kept fixed for the scans for relic density and direct detection cross section along with the mass of the Higgs bosons and dark matter candidate.

Parameters	$m_S^2$ (GeV <sup>2</sup> )	$\tan \beta$
Values	100-400000	5

TABLE IV. Range of relevant parameters varied for the scans involving the relic density and the direct detection cross section versus the dark matter mass,  $m_\chi$ . The other parameters are fixed as in Table III.

### Relic Density

In Fig. 5 we plot the relic density against the DM mass. We observe that the relic density of the complex scalar dark matter is satisfied at the resonance region corresponding to the lightest CP-even 125 GeV Higgs. One should note, however, that no funnel regions corresponding to heavy Higgs annihilation are observed for the parameter values fixed for the scans. However, these regions are accessible for large values of the portal couplings (close to the perturbativity limit). This is due to an interplay of the couplings and mass of the heavy Higgs while determining the cross sections during the relic density computation. In Fig. 1 there is a rapid change observed in the relic density near the  $m_\chi \simeq 75$  GeV where the thermal relic density is achieved. We focus on this region of light singlet dark matter region (defined as  $m_\chi \leq 100$  GeV). In the plot, we observe a funnel region near  $m_\chi \simeq m_h/2$  where the dark matter resonant annihilation occurs via the lightest CP-even Higgs with a mass of 125 GeV. The dominant processes contributing to the relic density in this region are  $b\bar{b}$  and sub-dominant contributions from  $WW$ . As one moves away from the funnel region, the  $WW$  mode starts dominating over  $b\bar{b}$ . This is due to the increasing phase space available to the

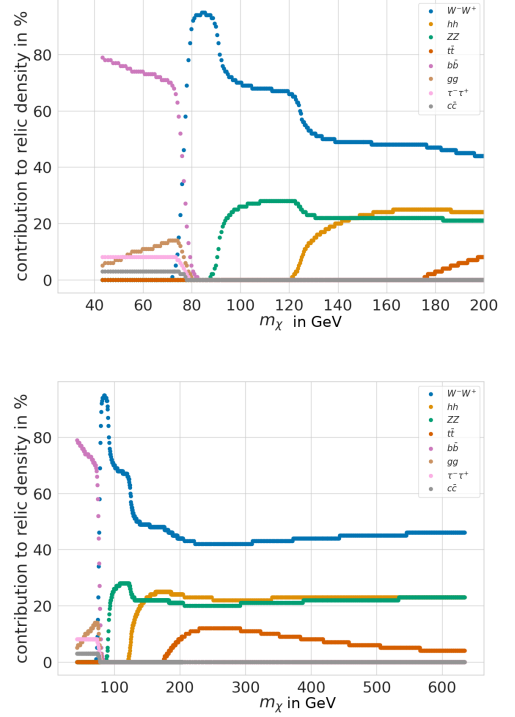


FIG. 6. The different processes contributing to the relic density.

final state particles due to the increase in mass of the dark matter candidate in the initial states. This continues up to masses close to  $m_W$  while near  $m_\chi \simeq m_W$ , the dominating mode is  $WW$ . As one increases  $m_\chi$  further the  $ZZ$  mode is now allowed once the  $m_\chi \simeq m_Z$ . In this region both the  $WW$  and  $ZZ$  modes contribute to the relic density computation. As  $m_\chi \simeq m_h$ , the di-Higgs channel opens up. Further, for  $m_\chi$  near the top mass, the  $t\bar{t}$  channel opens up.

We also look into the high mass region where a large portion of the parameter space remains underabundant up to  $m_\chi \simeq 480$  GeV after which the dark matter over-closes the universe. The processes contributing to the relic density are summarised in the Fig. 1. We observe that in these regions, as already discussed, the dominant modes are  $WW$ ,  $t\bar{t}$ ,  $hh$  and  $ZZ$ .

### Direct detection

The relevant constraints from direct detection cross section of dark matter arises from the spin-independent (SI) interactions. Fig. 7 shows the variation of the direct detection cross section against the dark matter mass  $m_\chi$ . We choose the parameters for the singlet and 2HDM parameters as in **BPA** and vary  $m_S^2$  to change the dark matter mass for  $\tan \beta = 5$ . We observe that the dark



matter direct detection stringently rules out dark matter masses less than 100 GeV while heavy dark matter remains allowed by current data.

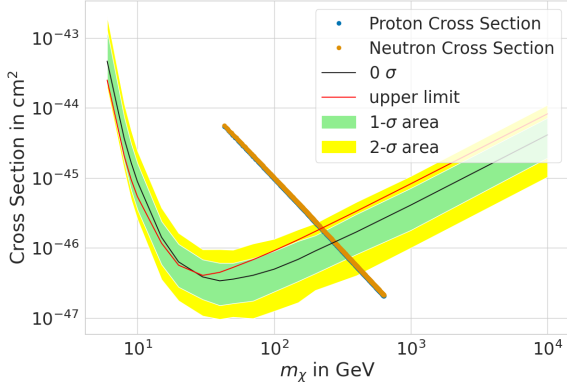


FIG. 7. Variation of the direct detection cross section against the mass of the dark matter candidate. The parameter  $m_S^2$  is varied in this plot in the range given in Table IV. The other input parameters are fixed as in Table III.

### Light singlet dark matter

There is a rapid change observed in the relic density near the  $Z$  boson threshold where the thermal relic density is achieved. We focus on this region of light singlet dark matter region (defined as  $m_\chi \leq 100$  GeV). Fig. 8 shows the variation of the relic density with the dark matter mass in this region. In this Higgs funnel region,

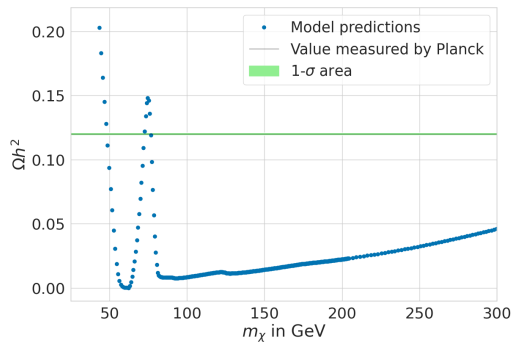


FIG. 8. Rapidly changing relic density in the low DM mass region. The parameter  $m_S^2$  is varied in this plot in the range given in Table IV. The other input parameters are fixed as in Table III.

the dominant processes contributing to the relic density are  $b\bar{b}$ ,  $g g$ ,  $\tau\bar{\tau}$ . As one moves to higher masses, the  $b\bar{b}$  mode decreases while the  $W W$  mode opens up as seen in

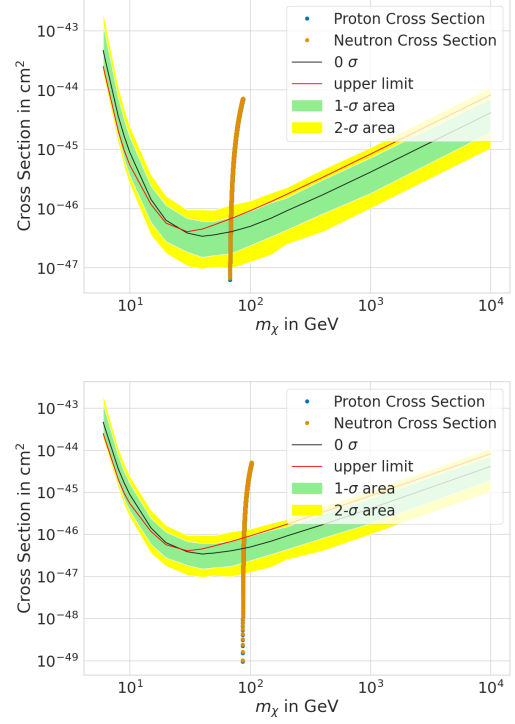


FIG. 9. Variation of the direct detection cross section versus the mass of the DM for varying  $\lambda'_2$  for two values of  $\tan \beta = 5, 20$ . The parameter varied in this plot is  $\lambda'_2$  as given in the Table V while the other parameters are same as listed in Table III.

the top panel of Fig. 6. However from Fig. 7 one can see that such a region is ruled out from the direct detection data. Therefore, we vary the other singlet parameters to see their effect on the direct detection parameters. The

Parameters	$\lambda'_2$	$\tan \beta$	$m_S^2 (\text{GeV}^2)$
Values	$10^{-4} - 0.1$	5, 20	4200

TABLE V. List of parameters for the variation of the relic density and the direct detection cross section for varying  $\lambda'_2$  for two values of  $\tan \beta$ . The other input parameters are chosen as in Table III.

strongest effect occurs of the portal coupling parameter  $\lambda'_2$  and  $\tan \beta$ . This can be explained from the nature of the coupling  $\lambda_{hSS^*}$  and  $\lambda_{HSS^*}$  (see eq. 40 and 43 respectively) that in the decoupling limit ( $\sin(\beta - \alpha) \simeq 1$ ) are functions of  $\lambda'_1$ ,  $\lambda'_2$  and  $\tan \beta$ . We observe this behaviour in Fig. 9 for two values of  $\tan \beta = 5, 20$ . We now scan over  $m_\chi$  as given in the Table VI and derive the allowed parameter space in Fig. 10.

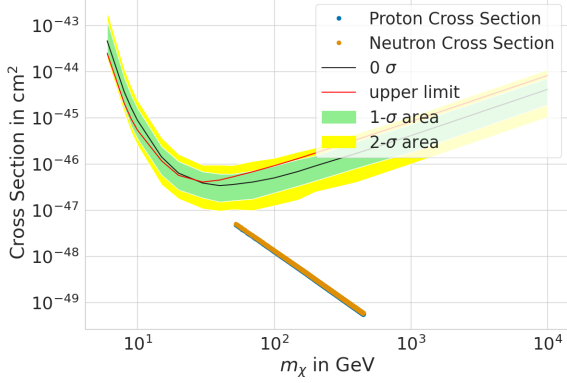


FIG. 10. Variation of the direct detection cross section versus  $m_\chi$  for  $\lambda'_2 = 0.001$  and  $\tan\beta = 12$ . The scan range for  $m_S^2$  is shown in Table VI while the other parameters are fixed as chosen as in Table III.

### Heavy singlet dark matter

From Fig. 6, we observe that the relic density remains underabundant up to  $m_\chi \leq 480$  GeV. From direct detection cross section constraint as shown in Figs. 7 and 10, we observe that the heavy dark matter masses are weakly constrained from experimental data.

Parameters	$m_S^2$ (GeV <sup>2</sup> )
Values	1000-200000

TABLE VI. The parameter ranges for the variation of direct detection cross section against the DM mass for  $\lambda'_2 = 0.001$  and  $\tan\beta = 12$ . The other parameters are fixed as in Table III.

In summary, we observe that the relic density is satisfied only around  $m_\chi \simeq 75$  GeV and  $\simeq 480$  GeV. Below 480 GeV, the DM relic density is mostly underabundant with the Higgs resonance region opening up near  $m_\chi \simeq 62$ -63 GeV. In this region, the dominant annihilation process of the DM is via the light 125 GeV Higgs with  $b\bar{b}$  being the dominant annihilation process. For heavier masses, the  $WW$  process is the dominant process, especially near the peak at  $m_\chi = 75$  GeV.

In the following section, we look into differences between real and complex scalar dark matter and choose some representative benchmark scenarios consistent with experimental constraints including dark matter, flavour physics, Higgs sector and collider constraints on heavy Higgs bosons.

### A. Distinction between real and complex scalar dark matter

In this section, we investigate the differences between a real and complex singlet scalar dark matter in the context of the 2HDMS. The similar comparison has been previously studied for the SM with singlet extensions[3] and for the 2HDM + scalar/pseudoscalar DM [56] in the context of collider signals.

The real scalar singlet extended 2HDM potential is

$$V_{RS} = M_{RS}^2 S^2 + \frac{\lambda_{R3}''}{4} S^4 + S^2 [\lambda_{1R}' \Phi_1^\dagger \Phi_1 + \lambda_{2R}' \Phi_2^\dagger \Phi_2] \quad (45)$$

The parameters are related to the parameters of the complex scalar potential, see Eq. 1 as

$$M_{RS}^2 = m_S^2 + m_S'^2, \quad (46)$$

$$\lambda_{3R}'' = \lambda_3'' + \frac{5}{3} \lambda_1'', \quad (47)$$

$$\lambda_{1R}' = \lambda_1' + 2\lambda_4', \quad (48)$$

$$\lambda_{2R}' = \lambda_2' + 2\lambda_5'. \quad (49)$$

In the limit of a real  $S$ , the complex scalar potential also reduces to the form of a real scalar potential for  $m_S'^2, \lambda_4', \lambda_5', \lambda_1'' = 0$ ,

$$M_{RS}^2 = m_S^2, \quad (50)$$

$$\lambda_{3R}'' = \lambda_3'', \quad (51)$$

$$\lambda_{1R}' = \lambda_1', \quad (52)$$

$$\lambda_{2R}' = \lambda_2'. \quad (53)$$

The result using the input parameters as listed in Table III is summarised in Table VII. The processes con-

Parameters	<b>BPB</b>
$M_{RS}^2$ (GeV <sup>2</sup> )	1.13e+05
$\lambda_{3R}''$	0.1
$\lambda_{1R}'$	0.042
$\lambda_{2R}'$	0.042
$m_\chi$ (GeV)	338.9
$m_h$ (GeV)	124.99
$m_H$ (GeV)	724.4
$m_A$ (GeV)	724.4
$m_{H^\pm}$ (GeV)	728.3
$m_\chi$	338.9
$\Omega h^2$	1.2
$\sigma_p^{SI}$ (in pb)	$7.67 \times 10^{-11}$
$\sigma_n^{SI}$ (in pb)	$7.90 \times 10^{-11}$

TABLE VII. The benchmark point in the real singlet extended 2HDM chosen for comparison with **BPA**. Although **BPB** is excluded from relic density, except at the Higgs resonance region, we choose **BPB** for comparison with **BPA**.

tributing to the relic density are  $WW$  (44%),  $hh$  (24%),  $ZZ$  (22%) and  $t\bar{t}$  (10%). In Table VIII we summarise both cases discussed so far, i.e. **BPA** for the complex DM and **BPB** for the real DM. We now perform a scan using the parameters listed in Table III (**BPA**) and vary  $m_S^2$ . We

choose similar masses for the dark matter candidate and the Higgs spectrum in both cases for comparison. We also ensure the same portal couplings  $\lambda'_1$ ,  $\lambda'_2$  and  $\lambda''_3$  in both real and complex cases. We observe that the relic den-

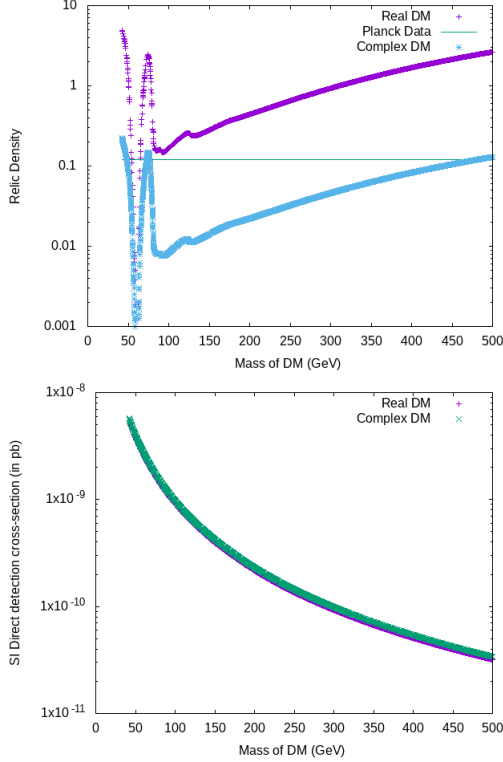


FIG. 11. Relic density (top) and SI (spin-independent) direct detection cross section (bottom) for real and complex DM. Although the real scalar DM case is excluded from relic density except at the Higgs resonance region, we show this plot for comparison with the complex scalar.

sity in the real scalar case is larger than in the complex scalar case and is excluded for this choice of parameters except at dark matter mass near the Higgs resonance region. However, we only chose this point **BPB** only for comparison with the complex scalar case to understand the differences between the two extensions.

Benchmark	Mass of DM (GeV)	$\Omega h^2$	$\sigma_p^{SI}$ (in pb)	$\sigma_n^{SI}$ (in pb)
<b>BPA</b> (complex DM)	338.0	0.059	$7.65 \times 10^{-11}$	$7.88 \times 10^{-11}$
<b>BPB</b> (real DM)	338.9	1.20	$7.67 \times 10^{-11}$	$7.90 \times 10^{-11}$

TABLE VIII. Comparison of the DM observables for complex and real scalar DM using the parameters listed in **BPA**. As already mentioned above, we choose **BPB** for comparison with **BPA** although it is excluded from relic density except at the Higgs resonance region.

In Fig. 11, we observe that the relic density for the same dark matter mass and with same portal couplings is much larger for the real DM case than the complex DM case. The extra contribution to the relic density arising

from the processes involving the extra portal and self-couplings of the dark matter leads to the different exclusion limits in the complex DM model. We also compare the direct detection cross section in the plot and observe no differences for the real limit of the complex case. This can be attributed to the fact that only the portal couplings  $\lambda'_1$  and  $\lambda'_2$  contribute in both cases for conserved DM number.

## B. Benchmarks

In this section, we present some representative benchmarks for 2HDMS consistent with all experimental constraints. We choose benchmark points for various dark matter masses in the light and heavy mass regions and include the possibility of the decay of the Higgs bosons into the dark matter candidate as summarised in Table IX. The model has been implemented in **SARAH-4.14.3**[55] and **SPheno-v4.0.4**[50] is utilized to obtain the benchmarks for the study. The tree-level unitarity constraints are checked using **SPheno-4.0.4**. In the following analysis **micrOMEGAs-v5.2.4**[48] is used to compute the tree-level relic density and the DM-nucleon cross sections. The constraints from the Higgs sector are checked using **HiggsBounds-v5**[57] and **HiggsSignals-v2**[58] at tree level. All benchmarks **BP1-BP3** lead to 125 GeV CP-even lightest Higgs as shown in Table IX.

Parameters	<b>BP1</b>	<b>BP2</b>	<b>BP3</b>
$\lambda_1$	0.23	0.1	0.23
$\lambda_2$	0.25	0.26	0.26
$\lambda_3$	0.39	0.10	0.2
$\lambda_4$	-0.17	-0.10	-0.14
$\lambda_5$	0.001	0.10	0.10
$m_{12}^2(\text{GeV}^2)$	$-1.0 \times 10^5$	$-1.0 \times 10^5$	$-1.0 \times 10^5$
$\lambda''_1$	0.1	0.1	0.1
$\lambda''_3$	0.1	0.1	0.1
$\lambda'_1$	0.042	0.04	2.0
$\lambda'_2$	0.042	0.001	0.01
$\lambda'_4$	0.1	0.1	0.1
$\lambda'_5$	0.1	0.1	0.1
$\tan \beta$	4.9	6.9	6.5
$m_h$ (GeV)	125.09	125.09	125.09
$m_H$ (GeV)	724.4	840.0	821.7
$m_A$ (GeV)	724.4	836.3	817.9
$m_{H^\pm}$ (GeV)	728.3	839.9	822.2
$m_{DM}$ (GeV)	338.0	76.7	323.6
$\Omega h^2$	0.058	0.119	0.05
$\sigma_p^{SI} \times 10^{10}$ (pb)	0.76	0.052	2.9
$\sigma_n^{SI} \times 10^{10}$ (pb)	0.78	0.054	3.1

TABLE IX. Relevant parameters of the benchmark used for the study. All mass parameters have units GeV except for  $m_{12}^2$  in  $\text{GeV}^2$ . The decimal points are rounded to the first decimal place for the masses and up to the third decimal place for the relic density, and the direct detection cross sections.

In benchmark **BP1** the relic density  $\Omega h^2 = 0.059$  and the direct detection cross section is,  $\sigma_p^{SI} = 7.55 \times 10^{-11}$

pb and  $\sigma_n^{SI} = 7.8 \times 10^{-11}$  pb. The benchmark **BP1** has an underabundant relic density but is consistent with the DM constraints from **PLANCK** as well as the **XENON1T** data for DM-nucleon scattering cross sections. The dominating annihilation channels are into  $W^+W^-$  (43%),  $hh$  (22%),  $ZZ$  (21%) and  $t\bar{t}$  (10%). This benchmark represents a heavy DM case, however with a 2HDM-like Higgs sector such that there are no appreciable decays of the heavy Higgs bosons to the dark matter.

**BP2** with  $m_\chi = 76.6$  GeV is another benchmark, addressing the light dark matter region also passing all constraints from the Higgs signal strength to ensure a phenomenologically viable benchmark point.

For both **BP1** and **BP2**, the dominant decay modes of the heavy Higgs bosons are summarised in Table X. In this case, the invisible branching ratio is suppressed and the Higgs bosons decay only with the 2HDM decay modes, i.e., completely indistinguishable from the 2HDM. In the presence of the dark matter, there are additional decay channels opening up for the heavy Higgs,  $H \rightarrow \chi\bar{\chi}$ . The presence of the invisible DM candidate in the final state ensures the presence of missing energy in the final state signal at colliders. Such signatures have been recently studied with the heavy Higgs as a portal to dark matter and its collider signals of mono-jets and VBF along with missing transverse energy at the LHC[16]. We consider this case in **BP3** where the allowed invisible branching of the Higgs bosons is  $\sim 4.8\%$  and all experimental constraints are respected. **BP3** is also a heavy DM benchmark point where the dark matter mass  $\sim 324$  GeV and is allowed by direct detection data at the 90% confidence level (CL), using **micrOmegas-v5.2.4**, see [48]. We also observe that the invisible decay branching of the heavy Higgs in **BP3** is severely constrained from direct detection searches.

Decay Channels	Branching ratios for		
	<b>BP1</b>	<b>BP2</b>	<b>BP3</b>
$H \rightarrow b\bar{b}$	0.14	0.29	0.24
$H \rightarrow t\bar{t}$	0.83	0.66	0.68
$H \rightarrow \tau\bar{\tau}$	0.02	0.45	0.04
$H \rightarrow \chi\bar{\chi}$	0.0	0.0	0.05
$A \rightarrow b\bar{b}$	0.12	0.27	0.27
$A \rightarrow t\bar{t}$	0.86	0.69	0.69
$A \rightarrow \tau\bar{\tau}$	0.02	0.04	0.04
$H^\pm \rightarrow t\bar{b}$	0.97	0.96	0.96
$H^\pm \rightarrow \tau\nu_\tau$	0.022	0.03	0.03

TABLE X. The branching ratios for the dominant decay modes of the heavy Higgs bosons for the benchmarks **BP1**, **BP2** and **BP3**. The branching ratios are rounded up to the second decimal place.

### C. Collider Analysis

In this section, we discuss the signatures of this model at the HL-LHC and at future  $e^+e^-$  colliders. As dis-

cussed in the previous section, the presence of the invisible decay of the Higgs bosons to the dark matter candidate is a source of missing energy signals at the colliders. Therefore, the direct production of heavy Higgs bosons and the consecutive decay of the heavy Higgs bosons into  $\chi$  visible SM particles can give rise to distinct signatures for this scenario as compared to the 2HDM-like scenario. We investigate the collider prospects of 2HDMS in the context of both  $\sqrt{s} = 14$  TeV LHC at the targeted integrated luminosity of  $3\text{--}4 \text{ ab}^{-1}$  and in future  $e^+e^-$  colliders up to  $\sqrt{s} = 3$  TeV and integrated luminosities  $5 \text{ ab}^{-1}$ .

#### Simulation details

We use **MG5\_aMC\_v3.1.1** [59, 60] to generate the parton level hard scattering processes for both signal and SM background. Hadronization and showering of the parton level events is performed using **Pythia-8**[61] while a fast detector simulation is performed using **Delphes-v3.4.1** [62–64] with the default Delphes card provided for ATLAS for the LHC study. For the  $e^+e^-$  study, we used the default Delphes card for the ILD detector based on [65]. We performed the signal-to-background analysis for LHC using **Delphes-v3.4.1** and **Madanalysis-v5**[66–70] for the electron-positron collider.

#### Prospects at LHC

The main processes contributing to neutral Higgs production are gluon fusion (mediated by the top quark loop), vector boson fusion (VBF) and associated Higgs production ( $Vh_i$ ),  $b\bar{b}h_i$ ,  $t\bar{t}h_i$ [6]. For the charged Higgs pair, the possible production channels are  $H^+H^-$  and  $W^\pm H^\mp$  [6]. At LHC Run 3 at  $\sqrt{s} = 14$  TeV, all possible Higgs production processes (including SM and BSM Higgs bosons) are summarised in Table XI for **BP1**. The current constraints on heavy Higgs bosons are summarised in [43, 44]. Projection studies of heavy Higgs bosons predict a mass reach of up to TeV for direct searches [71, 72] and indirect searches [73]. The HL-LHC is important to achieve the required luminosity to observe these channels and gain indirect insight into the BSM Higgs sector. The VBF and gluon fusion channel have been studied for the real singlet at LHC and are good discovery probes[16]. For the mass ranges of the heavy Higgs bosons considered in our study, the dominant production processes at  $\sqrt{s} = 14$  TeV LHC are:  $b\bar{b}H$ ,  $H + jj(ggF)$ ,  $VBF$ ,  $ZH$  and  $t\bar{t}H$ . The  $WH$  associated production is suppressed due to the suppressed couplings of the heavy Higgs bosons with respect to the SM couplings to the gauge bosons.

In the presence of the heavy Higgs  $H$  decaying to two dark matter candidates, one can obtain invisible momentum signatures in the final state. Keeping this in mind, one can look into the following final states:

- $1j \text{ (ISR)} + \cancel{E}_T$ [74]

Processes	cross section (in fb) at $\sqrt{s} = 14$ TeV		
	<b>BP1</b>	<b>BP2</b>	<b>BP3</b>
$h$ (ggF)	$29.3 \times 10^3$	$29.3 \times 10^3$	$29.3 \times 10^3$
$H$	22.61	5.238	6.632
$A$	35	8.58	10.8
$hjj$ (VBF)	$1.296 \times 10^3$	$1.265 \times 10^3$	$1.25 \times 10^3$
$Hjj$	1.843	1.845	0.56
$Ajj$	2.885	2.88	0.91
$Wh$	$1.148 \times 10^3$	$1.133 \times 10^3$	$1.134 \times 10^3$
$WH$	$1.195 \times 10^{-3}$	$1.11 \times 10^3$	$1.199 \times 10^{-3}$
$WA$	$4.3 \times 10^{-4}$	$5.9 \times 10^{-4}$	$5.7 \times 10^{-4}$
$Zh$	880.8	677.2	697.9
$ZH$	0.93	0.28	0.3408
$ZA$	3.99	1.41	1.69
$b\bar{b}h$	2534	2541	2541
$b\bar{b}H$	21.52	17.92	17.92
$b\bar{b}A$	23.39	18.9	19.04
$t\bar{t}h$	478.3	477.1	477.9
$t\bar{t}H$	0.199	0.0657	0.789
$t\bar{t}A$	0.255	0.0804	0.0983
$H^+H^-$	0.066	0.030	0.034
$W^\pm H^\mp$	102.4	3.45	4.14
$\chi\bar{\chi} + 1j$	0.006	0.0681	0.882

TABLE XI. The leading order (LO) cross section (in fb) for dominant processes for **BP1**, **BP2** and **BP3** before analysis for  $\sqrt{s} = 14$  TeV LHC.

- $2j + \cancel{E}_T$  [75]

We estimate the significance for the mono-jet and VBF channels using the cuts from an existing cut-and-count analyses performed in Ref.[16] for  $\sqrt{s} = 14$  TeV LHC.

#### Pre-selection cuts

The cuts used in this paper are summarised below. We choose the Delphes ATLAS card for reference.

- The leptons are reconstructed with a minimum transverse momentum,  $p_T > 10$  GeV and pseudorapidity  $|\eta| < 2.5$  while excluding the transitional pseudorapidity gap between the barrel and the end cap of the calorimeter  $1.37 < |\eta| < 1.52$ .
- Photons are reconstructed with  $p_T > 10$  GeV and  $|\eta| < 2.5$ .
- All jets are reconstructed using  $\Delta R = 0.4$  using the anti- $k_T$  algorithm and minimum  $p_T > 20$  GeV with pseudorapidity  $|\eta| < 2.5$ .

#### Signal Region A: $1j + \cancel{E}_T$

We estimate the signal events for the monojet +  $\cancel{E}_T$  channel using the SM background estimates in Ref. [16]. Using the kinematic cuts of  $p_T(j) > 250$  GeV and  $\cancel{E}_T >$

250 GeV, one obtains for **BP3** a signal efficiency of  $\sim 18\%$ . For the cut-and-count analysis, we obtain a signal significance of  $0.111\sigma$  excess at  $3 \text{ ab}^{-1}$  using gluon fusion production channel (at leading order (LO)).

#### Signal Region B: $2j + \cancel{E}_T$

We study the VBF topology for the signal region consisting of two forward jets and  $\cancel{E}_T$ . We follow the cuts in Ref.[16] for estimating the signal efficiency and use the background estimates from the paper. Using the signal cross section at LO, we get a signal efficiency of 4.5% for **BP3** and the signal significance is  $\sim 0.2 \sigma$  at  $3 \text{ ab}^{-1}$ .

Therefore, we observe that owing to the small invisible branching ratio and heavy Higgs masses  $\sim 820$  GeV (and hence small production cross section) in **BP3**, and the final states are inaccessible at the upcoming HL-LHC run. New machine learning techniques have shown an improvement for real singlet extended 2HDM as in Ref.[16] and may also be beneficial for the 2HDMS but is out of scope of our current work. Taking a different direction, we compare the reach in an  $e^+e^-$  collider and estimate the prospects of observing such a benchmark at the  $e^+e^-$  collider using a cut-and-count approach.

#### Prospects at $e^+e^-$ colliders

The cleaner environment compared to hadron colliders make the electron-positron linear collider attractive for precision studies of new physics. The International Linear Collider (ILC)[76], is a proposed  $e^+e^-$  collider with center-of-mass energies at the SM-like Higgs threshold ( $\sqrt{s} = 250$  GeV), top threshold ( $\sqrt{s} = 350$  GeV) and with further upgrades up to center of mass energies of  $\sqrt{s} = 500$  GeV up to  $\sqrt{s} = 1$  TeV with an annual luminosity of about  $\mathcal{L} = 500 \text{ fb}^{-1}$ . The ILC gains offers both the possibility of exploiting the polarization of the electron and positron beams leading to an increased background suppression, higher sensitivity to specific couplings and further new observables offering a rich window for unique phenomenology[77]. Other proposed  $e^+e^-$  colliders are CLIC [78, 79] with an energy upgrade up to  $\sqrt{s} = 3$  TeV, FCC-ee [80] and CEPC [81] with the latter having beam energies up to the  $t\bar{t}$  threshold.

For an  $e^+e^-$  collider, the main processes contributing to neutral Higgs production are  $Zh$ ,  $b\bar{b}h$ ,  $\nu\bar{\nu}h$ [6]. For the heavy scalar  $H$  and pseudoscalar  $A$ , the only relevant production channel which would be accessible up to  $\sqrt{s} = 3$  TeV are  $b\bar{b}H$ ,  $b\bar{b}A$ ,  $hA$ ,  $HA$ ,  $t\bar{t}H/A$  and  $\nu\bar{\nu}H/A$ . For the charged Higgs pair, the possible production channels are  $H^+H^-$  and  $W^\pm H^\mp$ [6]. One has the possibility of accessing the heavy Higgs bosons via the channels  $b\bar{b}H/A$ ,  $HA$  and  $t\bar{t}H/A$  at the CLIC with  $\sqrt{s} = 1.5(3)$  TeV.

As a representative study, we perform a signal-to-background analysis at a generic  $e^+e^-$  collider with  $\sqrt{s} = 3$  TeV and unpolarised electrons and positrons to

estimate the observability of these channels after background rejection for **BP3**. The presence of invisible dark matter in the final state manifests as missing energy in the final state along with visible SM-particles. For a detailed assessment, the inclusion of the polarized beams and for different luminosity running scenarios is required, which is postponed to a forthcoming study.

### Signals and backgrounds

From Table X, we observe that the dominant decay of the pseudoscalar is to a pair of top quarks and  $b$  quarks. For **BP3** a small fraction of the CP-even heavy Higgs decays to dark matter which manifests itself as missing energy at the collider. In such cases the dominant production processes  $HA$ ,  $b\bar{b}H$ ,  $t\bar{t}H$  and  $ZH$  lead to final states including (at least) two b-jets and missing energy while  $Hjj$  leads to a final state with two light jets associated with the missing energy with the latter having a VBF topology. On the other hand, the production channel  $\nu\bar{\nu}H$  state leads to a fully invisible state which in order to be probed requires an ISR photon against which the invisible system recoils. Besides, note that the heavy Higgs bosons ( $A$ ) also decay to a pair of tau leptons, therefore allowing the final state of  $2\tau + \cancel{E}_T$  from the  $HA$  production channel. Since the branching ratio of the  $A$  is dominantly into  $t\bar{t}$  followed by  $b\bar{b}$ , one expects final states involving at least  $2b + \cancel{E}_T$  to be dominant over the tau final states. In this work, we look into the prospects of observing signals including  $2b + \cancel{E}_T$ . Thus the relevant signal processes consist of the following production channels of the heavy CP-even Higgs,  $H$  such as

$$e^-e^+ \rightarrow HA, b\bar{b}H, t\bar{t}H$$

Contributions from  $HA$ ,  $b\bar{b}H$ ,  $t\bar{t}H$  lead to the final state of  $2b + \cancel{E}_T$  with the missing energy arising from  $H \rightarrow \chi\bar{\chi}$  while contributions from  $ZH$  production cross section is considerably suppressed at  $\sqrt{s} = 3$  TeV. We assume an integrated luminosity of  $\mathcal{L} = 5 \text{ ab}^{-1}$ .

### Pre-selection cuts

The cuts used for identifying the reconstructed objects after reconstruction with the default ILD card in **Delphes** based on Ref.[82] are summarised below and denoted as **C0**,

- Leptons are reconstructed with a minimum transverse momentum  $p_T > 10$  GeV and pseudorapidity  $|\eta| < 2.5$ .
- Photons are reconstructed with  $p_T > 10$  GeV and  $|\eta| < 2.5$ .
- All (b)-jets are identified with minimum  $p_T > 20$  GeV with pseudorapidity  $|\eta| < 3.0$ .

### Signal Region C: $2b + \cancel{E}_T$

We investigate the prospects of the final state consisting of two b-jets along with missing energy. Dominant contributions arise from

- $b\bar{b}$  (for misidentification of decay products of  $b$ -quark along with missing energy from  $b$  decays)
- $b\bar{b}\nu\bar{\nu}$  (including both on-shell and off-shell contribution from  $Z$  boson decay as well as  $\nu\bar{\nu}h$  contribution)
- $Z(\rightarrow b\bar{b})Z(\rightarrow \nu\bar{\nu})$
- $hZ$  ( $h \rightarrow b\bar{b}$ ,  $Z \rightarrow \nu\bar{\nu}$ )
- $t\bar{t}Z$ , ( $Z \rightarrow \nu\bar{\nu}$ ,  $t \rightarrow bW^+$ ) for misidentified leptons/jets from  $W$  bosons.
- Leptonic  $t\bar{t}$  for misidentified leptons or semi-leptonic  $t\bar{t}$  decays with missing energy arising from the  $b$  decaying leptonically.
- $WWZ$
- $ZZZ$

Benchmark	Process	cross sections (in fb)			
		250 GeV	500 GeV	1 TeV	3 TeV
<b>BP1</b>	$Zh$	237	56.68	12.75	1.361
	$b\bar{b}h$	36.61	8.918	1.985	0.1372
	$b\bar{b}H$	-	-	$1.355 \times 10^{-5}$	0.229
	$t\bar{t}h$	-	0.2583	2.121	0.5324
	$t\bar{t}H$	-	-	-	0.5666
	$HA$	-	-	-	0.71
	$\nu\nu h$	57.29	82.6	207.7	484.5
<b>BP2</b>	$Zh$	238.1	56.79	12.72	1.361
	$b\bar{b}h$	36.58	8.935	1.391	0.1275
	$b\bar{b}H$	-	-	0.2293	0.1769
	$t\bar{t}h$	-	0.2582	2.021	0.464
	$t\bar{t}H$	-	-	-	0.3906
	$\nu\nu h$	57.4	82.4	207.3	484.6
<b>BP3</b>	$Zh$	238.1	56.84	12.72	1.362
	$b\bar{b}h$	36.57	8.92	1.98	0.15
	$b\bar{b}H$	-	-	$1.35 \times 10^{-5}$	0.229
	$t\bar{t}h$	-	-	2.03	0.452
	$t\bar{t}H$	-	-	-	0.3906
	$HA$	-	-	-	0.7244
	$\nu\nu h$	57.28	82.6	207.8	483.6

TABLE XII. Unpolarised production cross sections for  $Zh$  and direct DM channels at a linear  $e^+e^-$  collider for **BP1**, **BP2** and **BP3** for  $\sqrt{s} = 250$  GeV, 500 GeV, 1 TeV and 3 TeV.

For the background processes, e.g.  $t\bar{t}$ ,  $t\bar{t}Z$  we generate the leptonic mode. For the other SM backgrounds, the  $Z(\rightarrow b\bar{b})Z(\rightarrow \nu\bar{\nu})$ ,  $h(\rightarrow b\bar{b})Z(\rightarrow \nu\bar{\nu})$ ,  $W(l\nu)W(l\nu)Z(\rightarrow b\bar{b})$  modes are generated. Since the signal benchmark **BP3** has a large dark matter mass ( $m_\chi \simeq 324$  GeV), with the DM candidate originating from the decay of the

SM Process	cross sections (in fb)
$ZZ$	1.54
$WW$	22.12
$b\bar{b}\nu\bar{\nu}$	40.84
$b\bar{b}$	10.17
$t\bar{t}$ (leptonic)	0.87
$t\bar{t}$ (semi-leptonic)	5.2
$t\bar{t}Z$	0.0149
$hZ$	0.23
$WWZ$	0.23
$ZZZ$	0.0151

TABLE XIII. Unpolarised background cross sections for SM backgrounds with leptonic decay models for  $t$  quarks,  $W$  boson, invisible decay of  $Z$ ,  $Z \rightarrow b\bar{b}$  and  $h \rightarrow b\bar{b}$ .

heavy Higgs  $H$  and a large mass gap between the parent and daughter particles, the signal sample has a large missing transverse energy as seen in Fig. 12 for the 2 b-jet final state. In order to generate the irreducible background final state  $b\bar{b}\nu\bar{\nu}$ , a large  $\cancel{E}_T (> 350 \text{ GeV})$  to tame the large the cross section of this background. The signal and background production cross section in the missing energy final state are summarised in Table XII and XIII. We now perform a signal-to-background analyses using the cuts **C1-C6** as follows,

- **C1:** The final state consists of two b-jets and no leptons or photons.
- **C2:** The leading b-jet has transverse momentum  $p_T > 100 \text{ GeV}$  and sub-leading b-jet has  $p_T > 80 \text{ GeV}$ . The hard  $p_T$  cuts on the b-jets help to reduce backgrounds from SM backgrounds from  $Z$  and  $h$  bosons.
- **C3:** The invariant mass of the two b-jets within the mass window  $80 \text{ GeV} < M_{b_1 b_2} < 130 \text{ GeV}$  is rejected to remove contributions from  $Z$  and  $h$  bosons.
- **C4:** Since the dark matter is heavy, we demand a large cut on the effective mass  $M_{eff} > 1.2 \text{ TeV}$  where  $M_{eff} = \sum_i(p_{T_i}) + \cancel{E}_T$ .
- **C5:** Furthermore, the large mass gap between the heavy Higgs and the dark matter allows for a large missing energy. We demand  $\cancel{E}_T > 650 \text{ GeV}$  on the final state which reduces the dominant SM backgrounds.
- **C6:** The  $\Delta\Phi$  between two b-jets is significantly different for the signal and background from  $b\bar{b}$  where the b-jets are mostly back-to-back. We demand  $\Delta\Phi(b_1, b_2) < 1.60$ . This also reduces the backgrounds from  $b\bar{b}$  as well as from  $t\bar{t}$  and  $t\bar{t}Z$  sharply.

The number of signal and background events after applying the cuts **C1-C6** (at  $\mathcal{L} = 5 \text{ ab}^{-1}$ ) are summarised in Table XIV. We observe that the large  $M_{eff}$  and  $\cancel{E}_T$  cut

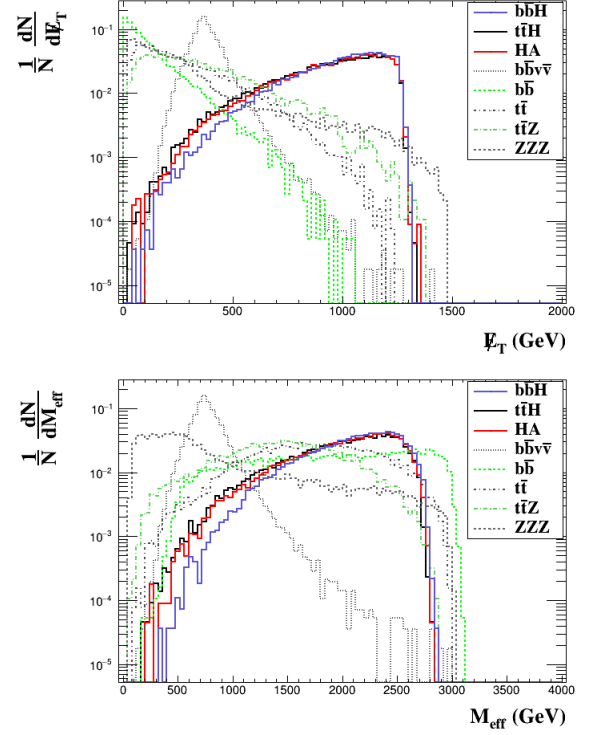


FIG. 12. Normalized distribution of missing transverse energy( $\cancel{E}_T$ ) and effective mass( $M_{eff}$ ) for signal vs. some backgrounds after cut **C1**. Concerning the  $t\bar{t}$  background the leptonic  $t\bar{t}$  contribution have been chosen.

are instrumental in reducing SM backgrounds sharply. Furthermore, the variable  $\Delta\Phi(b_1, b_2)$  also reduces contributions from  $b\bar{b}$  owing to the fact that the jets in the background are back to back while in the signal they are more collimated. It also reduces the backgrounds from  $t\bar{t}$  and  $t\bar{t}Z$  sharply which are also peaked towards higher values of  $\Delta\Phi$  as compared to the signal. We also plot the invariant mass of the two b-jets in Fig. 13 and observe that the SM backgrounds from  $Z$  and  $h$  are peaked at the resonance masses but for the signal the peak is broader since the parent particle is heavy. However, the irreducible background  $b\bar{b}\nu\bar{\nu}$  has a similar shape compared to the signal. Therefore, excluding the mass window  $80 \text{ GeV} < M_{b_1 b_2} < 130 \text{ GeV}$ , removes the resonant backgrounds from  $Z$  and  $h$  bosons, however with retaining backgrounds involving b-jets associated with neutrinos and also from  $t\bar{t}$  associated backgrounds.

We discuss the signal significance only for unpolarised electron and positron beams. The statistical significance ( $\mathcal{S}$ ) of the signal ( $s$ ) over the total SM background ( $b$ ) is calculated using [83, 84]

$$\mathcal{S} = \sqrt{2 \times \left[ (s+b) \ln\left(1 + \frac{s}{b}\right) - s \right]}. \quad (54)$$

where  $s$  and  $b$  are the total signal and background event numbers after the cuts **C1-C6**. We use this expression



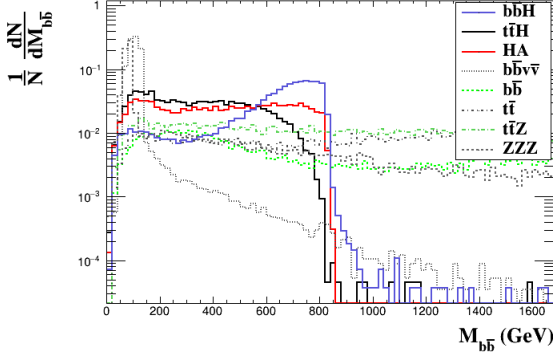


FIG. 13. Normalized distribution of the invariant mass of the two b-jets for signal vs. background after cut **C1**. Concerning the  $t\bar{t}$  background the leptonic  $t\bar{t}$  contribution have been chosen.

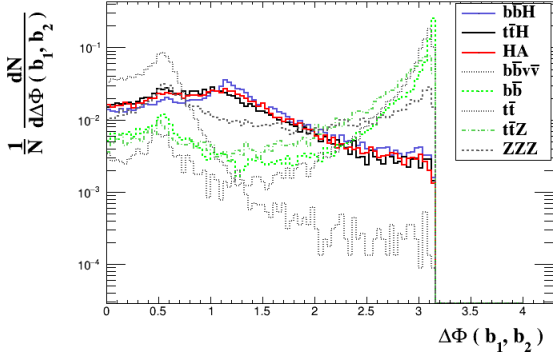


FIG. 14. Normalized distribution of  $\Delta\Phi$  separation between the two final state b-jets after cut **C1**. Concerning the  $t\bar{t}$  background the leptonic  $t\bar{t}$  contribution have been chosen.

for the statistical significance since the background events are not overwhelmingly large compared to the signal and the limit  $b \gg s$  is not fully accurate.<sup>4</sup> We observe that for **BP3**, although the invisible decay branching ratio of the heavy Higgs is small, i.e.  $H \rightarrow \chi\bar{\chi} \sim 4.8\%$ , one can obtain  $\sim 4\sigma$  signal at the integrated luminosity of  $5 \text{ ab}^{-1}$ . Note that we have used unpolarised incoming beams for this study. It is well known that the use of a right-handed electron and left-handed positron beam polarization can significantly suppress SM backgrounds [77] and can be effectively used to improve the signal significance as proposed at the upcoming ILC with the possibility of achieving beam polarizations (80%, 30–60%) for  $(e^-, e^+)$ . With the CLIC experiment potentially targeting higher center-of-mass energies but with electron

<sup>4</sup> In the limit  $b \gg s$ , Eq. 54 reduces to  $S = \frac{s}{\sqrt{b}} \simeq 4.21 \sigma$  ( for  $S = \frac{s}{\sqrt{s+b}} \simeq 3.63 \sigma$ ).

Process	C0	C1	C2	C3	C4	C5	C6
$bbH$	115	32	27	26	26	25	21
$t\bar{t}H$	101	22	13	12	12	11	10
$HA$	170	38	28	24	24	22	20
<b>BP3</b>	51						
$bb\nu\bar{\nu}$	204200	35159	15738	2040.9	330.3	147.6	124.3
$b\bar{b}$	50850	9514.5	8432.5	8387.2	6697.5	65.6	4.07
$ZZZ$	75	10.89	3.75	3.07	1.5	0.51	0.28
$WWZ$	1163	42.8	3.14	1.1	0.14	0.02	-
$t\bar{t}Z$	74	7.1	5.68	5.6	4.04	0.71	0.35
$t\bar{t}$ (semi-leptonic)	25955	3846.1	2843.9	2818.8	2500.6	338.5	16.61
$t\bar{t}$ (leptonic)	4328	565.4	481.5	478.3	401.9	29.65	1.13
$hZ$	110620	0.55	0.28	0.28	-	-	-
$hZ$	1131	6.8	1.26	0.023	-	-	-
$ZZ$	7699	167.9	42.81	13.0	-	-	-
Total background	146.4						
Significance	3.99						

TABLE XIV. The cut-flow table showing the change in the number of events for the benchmark **BP3** for unpolarised electron and positron beams at  $\sqrt{s} = 3 \text{ TeV}$  at  $\mathcal{L} = 5 \text{ ab}^{-1}$ . The cuts (**C0-C6**) are defined in the text in Sec. VC. The '-' denotes results with less than 1 event at an integrated luminosity  $\mathcal{L} = 5 \text{ ab}^{-1}$ .

polarization only, one may hope to further enlarge the discovery range.

## VI. CASE B: TWO COMPONENT FRAMEWORK

In this section, we discuss the impact of imposing the constraints on the singlet for not obtaining a  $vev$  (as discussed in sec. III A such that  $m_{h_s}^2 > 0$  and  $m_{a_s}^2 > 0$  to avoid spontaneous symmetry breaking of  $Z_2'$ ) and work in the two-component form where both  $h_s$  and  $a_s$  contribute to the relic density with the lightest one being the dark matter candidate. From sec. II, recall eq. 23 and 24 for the squared-masses of  $h_s$  and  $a_s$  are

$$m_{h_s}^2 = \frac{1}{2}(m_S^2 + m_{S'}^2 + (\lambda_1' + 2\lambda_4')v_1^2 + (\lambda_2' + 2\lambda_5')v_2^2),$$

$$m_{a_s}^2 = \frac{1}{2}(m_S^2 - m_{S'}^2 + (\lambda_1' - 2\lambda_4')v_1^2 + (\lambda_2' - 2\lambda_5')v_2^2)$$

and eq. 25

$$\Delta^2 = |m_{h_s}^2 - m_{a_s}^2| = m_{S'}^2 + 2\lambda_4'v_1^2 + 2\lambda_5'v_2^2$$

where  $\Delta^2$  is the squared mass difference of the two dark states. Recall, from sec. II, eq. 27–30, the couplings of  $h_s$  and  $a_s$  with the Higgs bosons are

$$\begin{aligned}\lambda_{hh_s h_s} &= -2v(\lambda_1' + 2\lambda_4') \cos \beta, \\ \lambda_{Hh_s h_s} &= -2v(\lambda_2' + 2\lambda_5') \sin \beta, \\ \lambda_{ha_s a_s} &= -2v(\lambda_1' - 2\lambda_4') \cos \beta, \\ \lambda_{Ha_s a_s} &= -2v(\lambda_2' - 2\lambda_5') \sin \beta.\end{aligned}$$

The portal couplings  $\lambda_1', \lambda_2', \lambda_4'$  and  $\lambda_5'$  are instrumental in determining the coupling of the Higgs bosons to the



dark sector particles and affect the DM phenomenology crucially, while the quartic couplings  $\lambda_1''$  and  $\lambda_3''$  do not affect the DM observables. For the rest of the study,  $m_{DM_1}$  and  $m_{DM_2}$  refer to the mass of the lightest and heaviest dark sector particle, respectively, and we choose  $\lambda_4' = \lambda_5'$  for simplicity. Fig. 15 shows the variation of the relic density versus the mass of the lightest dark sector particle, i.e.,  $m_{DM_1}$  with the possibility of the lightest dark sector particle being  $h_s$  (black points) (with  $Z_{12} = 0$ ) or  $a_s$  (yellow points) (with  $Z_{12} = 1$ ). Note that  $Z$  is an identity matrix denoting the mixing in the  $h_s - a_s$  sector. Hence,  $Z_{12} = 0$  refers to the case where  $h_s$  is the lightest dark sector particle while  $Z_{12} = 1$  refers to  $a_s$  as the lightest dark sector particle, since no mixing term  $h_s a_s$  is allowed by the symmetries of the scalar potential. The relic den-

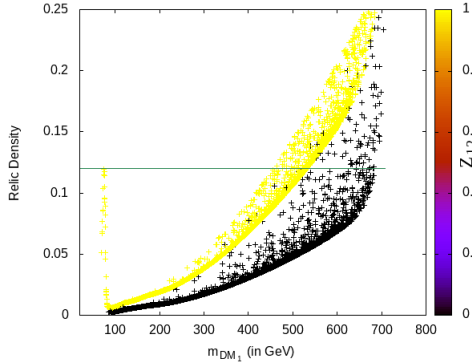


FIG. 15. Distribution for the relic density vs. the mass of the lightest DM candidate with the panel denoting the dark matter mixing matrix component ( $Z_{12}$ ) of the DM sector in the basis ( $h_s - a_s$ ). The yellow points indicate  $Z_{12} = 1$  corresponding to the lightest dark sector particle being  $h_s$  while the black points correspond to  $Z_{12} = 0$  with  $a_s$  as the lightest dark sector particle.

sity includes contributions from both  $h_s$  and  $a_s$ . Due to the U(1) symmetry breaking terms  $\lambda_4'$  and  $\lambda_5'$ ,  $h_s$  and  $a_s$  are not mass degenerate but there exists a mass splitting  $\Delta$ . For positive U(1) breaking terms,  $a_s$  is the DM candidate while for negative values of the portal couplings,  $h_s$  is the DM candidate. The difference in the nature of the relic density when  $h_s$  is the DM candidate compared to the case where  $a_s$  is the dark matter candidate in the figure arises from the difference in the masses and couplings of  $h_s$  and  $a_s$  to the Higgs bosons. Next, we look into the mass plane of the dark sector particles, i.e.,  $m_{DM_1}$  and  $m_{DM_2}$ , see Fig. 16 for two values of  $\tan \beta = 5, 10$ . We ensure that the upper limit of relic density is respected for the scan points as seen in Fig. 16 (left panels). For  $\tan \beta = 5$  (left), we observe stringent constraints on the parameter space from the spin-independent direct detection cross section which is alleviated for a higher value of  $\tan \beta = 10$  (right), where the allowed parameter space includes a larger fraction of points extending into lower dark matter masses.

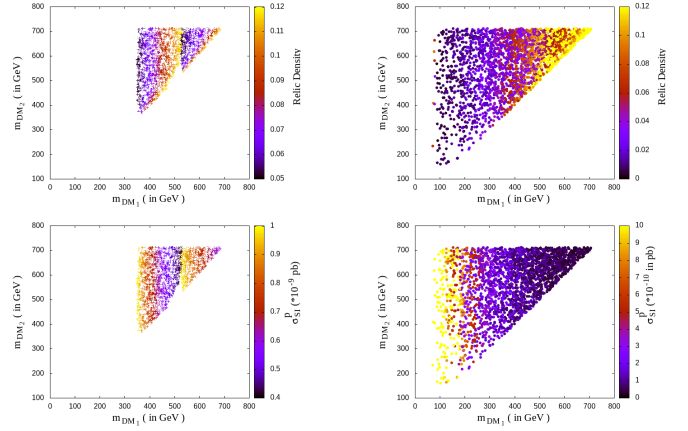


FIG. 16. Variation of the masses of the two DM candidates satisfying relic density and direct detection cross section for  $\tan \beta = 5$  (left) and 10 (right).

### A. Collider Analyses

Now we discuss the collider phenomenology of representative benchmarks satisfying the  $v_s = 0$  constraint as well as the experimental constraints from **HiggsBounds** and **HiggsSignals**. The benchmark scenarios, generated using **SPheno-v4.0.5**, are listed in Table XV. We choose the benchmark examples with the Higgs sector as in **BP3** and rescale the results from the collider analyses for the signal region C for **BP4** and **BP5** using the new branching fractions to the lightest dark matter candidate. The results for the cut-flow of the number of events are summarised in Table XVI for an unpolarised  $e^+e^-$  collider with  $\sqrt{s} = 3$  TeV. We observe that both benchmark scenarios are observable with an excess of  $3\sigma$  and  $6\sigma$  at the linear collider at 3 TeV, for **BP5** and **BP4**, respectively which differ in the invisible branching of the heavy CP-even Higgs with a larger branching fraction of 7.6% of **BP4** as compared to **BP5** as well as **BP3**. The statistical significance ( $\mathcal{S}$ ) is given in Table VI A.

## VII. SUMMARY AND CONCLUSIONS

We consider the Type II Two Higgs Doublet model extended with a complex singlet scalar (2HDMS), motivated to address several open issues in nature. The softly broken  $Z_2$ -symmetric 2HDM scalar potential is augmented with a complex scalar symmetric under  $Z_2'$ , stabilizing the dark matter candidate. Since the complex scalar singlet does not develop a vacuum expectation value, the Higgs spectrum is the same as in the 2HDM. In the CP-conserving scenario, the CP-even Higgs bosons act as a portal to the dark matter. We explore the parameter space allowed by current experimental data from dark matter, flavour physics and collider constraints from the SM-like Higgs as well as searches for the heavy Higgs

Parameters	BP4	BP5
$\lambda_1$	0.23	0.23
$\lambda_2$	0.26	0.26
$\lambda_3$	0.39	0.39
$\lambda_4$	-0.17	-0.17
$\lambda_5$	0.001	0.001
$m_{12}^2(\text{GeV}^2)$	$1.01 \times 10^5$	$1.01 \times 10^5$
$\tan \beta$	6.5	6.5
$m_h(\text{GeV})$	124.9	124.9
$m_H(\text{GeV})$	821.6	821.6
$m_A(\text{GeV})$	821.5	821.5
$m_{H^\pm}(\text{GeV})$	824.6	824.6
$m_{a_s}(\text{GeV})$	96.48	241.31
$m_{h_s}(\text{GeV})$	344.36	243.36
$\text{BR}(H \rightarrow a_s a_s)$	$7.6 \times 10^{-2}$	$3.3 \times 10^{-2}$
$\Omega h^2$	$1.15 \times 10^{-1}$	$1.53 \times 10^{-3}$
$\sigma_p^{SI}(\text{pb})$	$8.12 \times 10^{-10}$	$9.03 \times 10^{-12}$
$\sigma_n^{SI}(\text{pb})$	$8.41 \times 10^{-10}$	$9.56 \times 10^{-12}$

TABLE XV. Relevant parameters of the benchmark used for the study. All mass parameters have units GeV except for  $m_{12}^2$  in  $\text{GeV}^2$ .

Process	C1	C2	C3	C4	C5	C6
$bbH$	51	43	41	41	39	32
$t\bar{t}H$	35	20	18	18	16	16
$HA$	59	45	39	39	35	31
<b>BP4</b>	79					
$bbH$	25	21	20	20	19	16
$t\bar{t}H$	17	10	9	9	8	8
$HA$	29	22	19	19	17	15
<b>BP5</b>	39					
$bb\nu\bar{\nu}$	35159	15738	2040.9	330.3	147.6	124.3
$b\bar{b}$	9514.5	8432.5	8387.2	6697.5	65.6	4.07
$ZZZ$	10.89	3.75	3.07	1.5	0.51	0.28
$WWZ$	42.8	3.14	1.1	0.14	0.02	-
$t\bar{t}Z$	7.1	5.68	5.6	4.04	0.71	0.35
$t\bar{t}(\text{sl})$	3846.1	2843.9	2818.8	2500.6	338.5	16.61
$t\bar{t}(\text{dl})$	565.4	481.5	478.3	401.9	29.65	1.13
$WW$	0.55	0.28	0.28	-	-	-
$hZ$	6.8	1.26	0.023	-	-	-
$ZZ$	167.9	42.81	13.0	-	-	-
Total	146.4					

TABLE XVI. The cut-flow table showing the change in the number of events for the unpolarised electron and positron at  $\sqrt{s} = 3 \text{ TeV}$  at  $\mathcal{L} = 5 \text{ ab}^{-1}$ . The cuts (**C1-C6**) are defined in the text in Sec. V C.

bosons. We observe that direct detection results stringently constrain the parameter space and require low values of  $\lambda_2'$ . Furthermore, we compare our results with the real singlet extended 2HDM and observe that the contributions to the relic density are much larger for the complex scalar DM over the real scalar DM while the direct detection cross section are very similar in both extensions.

The presence of the singlet also leads to new decay modes for the Higgs bosons namely into a pair of dark

Benchmarks	$\mathcal{S}$
BP4	6.04
BP5	3.09

TABLE XVII. The statistical significance for benchmarks **BP4** and **BP5** at  $\sqrt{s} = 3 \text{ TeV}$  and luminosity  $\mathcal{L} = 5 \text{ ab}^{-1}$ .

matter particles. Such a final state will lead to the signature of missing energy at colliders. We choose a representative benchmark **BP3** with  $m_H \simeq 820 \text{ GeV}$  consistent with all experimental data in order to demonstrate the prospects of observing such a signal at HL-LHC and at future  $e^+e^-$  colliders. In this case, the constraints from direct detection data as well as the competing fermionic decays of the heavy Higgs bosons stringently constrain the invisible decay  $H \rightarrow \chi\bar{\chi} \simeq 4.8\%$ . Due to the small branching fraction and the heavy mass of  $H$ , rather low cross sections HL-LHC are obtained. However, one has a better handle on the background at an  $e^+e^-$  collider due to the precise initial energy and the clean environment as compared to the HL-LHC. We perform a signal-to-background analyses at the  $e^+e^-$  collider with  $\sqrt{s} = 3 \text{ TeV}$  with unpolarised beams and derive that the  $2b + \cancel{E}_T$  channel is observable with a  $= 3.99\sigma$  significance at an integrated luminosity  $\mathcal{L} = 5 \text{ ab}^{-1}$ . One should note, however, that still beam polarization has not been applied for the current study, which will lead to higher significance even for BP3.

We also study the impact of theoretical constraints such as the conditions for imposing no  $vev$  on the singlet scalar on the dark matter phenomenology and observe some benchmark examples within the reach at a future  $e^+e^-$  factory. However, we have not yet included beam polarization effects yet. We leave a further optimized study for the linear collider for a future study.

## ACKNOWLEDGEMENTS

JD and GMP acknowledge support by the Deutsche Forschungsgemeinschaft (DFG, German Research Foundation) under Germany's Excellence Strategy EXC 2121 "Quantum Universe"- 390833306. The authors thank G.Belanger, A.Pukhov from the micrOMEGAs team, J.Heisig, O.Mattalea and C.Arina from the maDDM team for helpful correspondence. The authors also thank H.Bahl, S.Heinemeyer, C.Li, S. Paasch, T.Stefaniak and G.Weiglein for helpful discussions and help with HiggsBounds and HiggsSignals.

## APPENDIX

### Analytical computation of direct detection cross section

We compute the direct detection cross section. The DM-quark amplitude of the tree level Feynman diagram

Fig. 4 for zero momentum transfer is

$$\mathcal{M} = \sum_{h_i} \lambda_{h_i SS^*} \frac{1}{-m_{h_i}^2} \lambda_{h_i q \bar{q}}, \quad (55)$$

where  $h_i = h, H$ . Recall,

$$\lambda_{h SS^*} = \frac{v}{\sqrt{1 + \tan^2 \beta}} (\lambda'_1 \sin \alpha - \lambda'_2 \tan \beta \cos \alpha),$$

$$\lambda_{H SS^*} = -\frac{v}{\sqrt{1 + \tan^2 \beta}} (\lambda'_1 \cos \alpha - \lambda'_2 \tan \beta \sin \alpha)$$

and

$$\lambda_{h_i q \bar{q}} = \frac{m_q}{v} C^{h_i}$$

is the Yukawa coupling of the quark to the Higgs bosons. For Type II 2HDM[6] the Higgs couplings to the fermions are summarised in Table XVIII.

Higgs bosons	$C_u$	$C_d$	$C_s$
$h$	$\cos \alpha / \sin \beta$	$-\sin \alpha / \cos \beta$	$-\sin \alpha / \cos \beta$
$H$	$\sin \alpha / \sin \beta$	$\cos \alpha / \cos \beta$	$\cos \alpha / \cos \beta$

TABLE XVIII. The couplings of the quarks in Type II 2HDM[6].

In order to compute the DM-nucleon amplitude, the nucleon form factors  $f_N$  need to be folded into the quark-DM amplitude  $\mathcal{M}$ . The form factors  $f^N$  for  $N = p, n$  are[13]

$$f_N = \frac{m_N}{2m_\chi} \left( \sum_{q=u,d,s} f_{Tq}^N \frac{\mathcal{M}}{m_q} + \frac{2}{27} f_{TG}^N \sum_{q=c,b,t} \frac{\mathcal{M}}{m_q} \right), \quad (56)$$

where the first term is due to the contribution of the light valence quarks and the second term due to the gluonic form factor  $f_{TG}^N$  defined as,

$$f_{TG}^N = 1 - \sum_{q=u,d,s} f_{Tq}^N. \quad (57)$$

Folding in the form factors above and the phase space of the DM-nucleon scattering, the DM-nucleon cross sections for the proton and neutron are[13, 85],

$$\sigma_{SI}^p = \frac{4\mu_N^2}{\pi} (Z f_p)^2 \quad (58)$$

and

$$\sigma_{SI}^n = \frac{4\mu_N^2}{\pi} ((A - Z) f_n)^2 \quad (59)$$

where  $\mu_N = \frac{m_\chi m_N}{(m_\chi + m_N)}$  for nucleon  $N = p, n$ .

- 
- [1] Vernon Barger, Paul Langacker, Mathew McCaskey, Michael Ramsey-Musolf, and Gabe Shaughnessy. Complex Singlet Extension of the Standard Model. *Phys. Rev. D*, 79:015018, 2009.
- [2] James M. Cline, Kimmo Kainulainen, Pat Scott, and Christoph Weniger. Update on scalar singlet dark matter. *Phys. Rev. D*, 88:055025, 2013. [Erratum: *Phys. Rev. D* 92, 039906 (2015)].
- [3] Hongyan Wu and Sibor Zheng. Scalar Dark Matter: Real vs Complex. *JHEP*, 03:142, 2017.
- [4] Avirup Ghosh, Deep Ghosh, and Satyanarayan Mukhopadhyay. Cosmology of complex scalar dark matter: Interplay of self-scattering and annihilation. *Phys. Rev. D*, 104(12):123543, 2021.
- [5] E. Aprile et al. Dark Matter Search Results from a One Ton-Year Exposure of XENON1T. *Phys. Rev. Lett.*, 121(11):111302, 2018.
- [6] G.C. Branco, P.M. Ferreira, L. Lavoura, M.N. Rebelo, Marc Sher, and Joao P. Silva. Theory and phenomenology of two-Higgs-doublet models. *Phys. Rept.*, 516:1–102, 2012.
- [7] Nilendra G. Deshpande and Ernest Ma. Pattern of Symmetry Breaking with Two Higgs Doublets. *Phys. Rev. D*, 18:2574, 1978.
- [8] Xiao-Gang He, Tong Li, Xue-Qian Li, Jusak Tandean, and Ho-Chin Tsai. Constraints on Scalar Dark Matter from Direct Experimental Searches. *Phys. Rev. D*, 79:023521, 2009.
- [9] B. Grzadkowski and P. Osland. Tempered Two-Higgs-Doublet Model. *Phys. Rev. D*, 82:125026, 2010.
- [10] Chien-Yi Chen, Michael Freid, and Marc Sher. Next-to-minimal two Higgs doublet model. *Phys. Rev. D*, 89(7):075009, 2014.
- [11] Yi Cai and Tong Li. Singlet dark matter in a type II two Higgs doublet model. *Phys. Rev. D*, 88(11):115004, 2013.
- [12] Lei Wang and Xiao-Fang Han. A simplified 2HDM with a scalar dark matter and the galactic center gamma-ray excess. *Phys. Lett. B*, 739:416–420, 2014.
- [13] Aleksandra Drozd, Bohdan Grzadkowski, John F. Gunion, and Yun Jiang. Extending two-Higgs-doublet models by a singlet scalar field - the Case for Dark Matter. *JHEP*, 11:105, 2014.
- [14] Xiao-Gang He and Jusak Tandean. New LUX and PandaX-II Results Illuminating the Simplest Higgs-

- Portal Dark Matter Models. *JHEP*, 12:074, 2016.
- [15] Margarete Muhlleitner, Marco O. P. Sampaio, Rui Santos, and Jonas Wittbrodt. The N2HDM under Theoretical and Experimental Scrutiny. *JHEP*, 03:094, 2017.
- [16] Atri Dey, Jayita Lahiri, and Biswarup Mukhopadhyaya. LHC signals of a heavy doublet Higgs as dark matter portal: cut-based approach and improvement with gradient boosting and neural networks. *JHEP*, 09:004, 2019.
- [17] Sebastian Baum and Nausheen R. Shah. Two Higgs Doublets and a Complex Singlet: Disentangling the Decay Topologies and Associated Phenomenology. 2018. [JHEP12,044(2018)].
- [18] Thomas Biekötter and María Olalla Olea-Romacho. Reconciling Higgs physics and pseudo-Nambu-Goldstone dark matter in the S2HDM using a genetic algorithm. *JHEP*, 10:215, 2021.
- [19] S. Heinemeyer, C. Li, F. Lika, G. Moortgat-Pick, and S. Paasch. A 96 GeV Higgs Boson in the 2HDM plus Singlet. 12 2021.
- [20] Cesar Bonilla, Dorota Sokolowska, Neda Darvishi, J. Lorenzo Diaz-Cruz, and Maria Krawczyk. IDMS: Inert Dark Matter Model with a complex singlet. *J. Phys. G*, 43(6):065001, 2016.
- [21] M. Muhlleitner, J. Müller, S. L. Williamson, and J. Wittbrodt. The CN2HDM. 10 2021.
- [22] Kristjan Kannike, Kaius Loos, and Martti Raidal. Gravitational wave signals of pseudo-Goldstone dark matter in the  $\mathbb{Z}_3$  complex singlet model. *Phys. Rev. D*, 101(3):035001, 2020.
- [23] A. R. Zhitnitsky. On Possible Suppression of the Axion Hadron Interactions. (In Russian). *Sov. J. Nucl. Phys.*, 31:260, 1980.
- [24] Michael Dine, Willy Fischler, and Mark Srednicki. A Simple Solution to the Strong CP Problem with a Harmless Axion. *Phys. Lett. B*, 104:199–202, 1981.
- [25] G. C. Dorsch, S. J. Huber, T. Konstandin, and J. M. No. A Second Higgs Doublet in the Early Universe: Baryogenesis and Gravitational Waves. *JCAP*, 05:052, 2017.
- [26] Waleed Abdallah, Raj Gandhi, and Samiran Roy. Two-Higgs doublet solution to the LSND, MiniBooNE and muon  $g-2$  anomalies. *Phys. Rev. D*, 104(5):055028, 2021.
- [27] Venus Keus, Niko Koivunen, and Kimmo Tuominen. Singlet scalar and 2HDM extensions of the Standard Model: CP-violation and constraints from  $(g-2)_\mu$  and  $eEDM$ . *JHEP*, 09:059, 2018.
- [28] Atri Dey and Jayita Lahiri. Collider Signatures of Type-X 2HDM + scalar singlet dark matter at HL-LHC. 12 2021.
- [29] Andi Hektor, Kristjan Kannike, and Luca Marzola. Muon  $g-2$  and Galactic Centre  $\gamma$ -ray excess in a scalar extension of the 2HDM type-X. *JCAP*, 10:025, 2015.
- [30] Juhi Dutta, Gudrid Moortgat-Pick, Cheng Li, Farah Tabira Sheikh, and Julia Ziegler. *Work in Progress*.
- [31] <https://pdg.lbl.gov/2022/tables/rpp2022-sum-gauge-higgs-bosons.pdf>.
- [32] Combination of searches for invisible Higgs boson decays with the ATLAS experiment. 10 2020.
- [33] Albert M Sirunyan et al. Search for invisible decays of a Higgs boson produced through vector boson fusion in proton-proton collisions at  $\sqrt{s} = 13$  TeV. *Phys. Lett. B*, 793:520–551, 2019.
- [34] J.P. Lees et al. Precision Measurement of the  $B \rightarrow X_s \gamma$  Photon Energy Spectrum, Branching Fraction, and Direct CP Asymmetry  $A_{CP}(B \rightarrow X_{s+d} \gamma)$ . *Phys.Rev.Lett.*, 109:191801, 2012.
- [35] R. Aaij et al. Measurement of the  $B_s^0 \rightarrow \mu^+ \mu^-$  branching fraction and search for  $B^0 \rightarrow \mu^+ \mu^-$  decays at the LHCb experiment. *Phys.Rev.Lett.*, 111:101805, 2013.
- [36] Serguei Chatrchyan et al. Measurement of the  $B(s)$  to  $\mu^+ \mu^-$  branching fraction and search for  $B^0$  to  $\mu^+ \mu^-$  with the CMS Experiment. *Phys.Rev.Lett.*, 111:101804, 2013.
- [37] <https://pdg.lbl.gov/2020/reviews/rpp2020-rev-g-2-muon-anom-mag-moment.pdf>.
- [38] Particle Data Group and P A et.al Zyla. Review of Particle Physics. *Progress of Theoretical and Experimental Physics*, 2020(8), 08 2020. 083C01.
- [39] N. Aghanim et al. Planck 2018 results. VI. Cosmological parameters. *Astron. Astrophys.*, 641:A6, 2020.
- [40] M. Ackermann et al. Constraining Dark Matter Models from a Combined Analysis of Milky Way Satellites with the Fermi Large Area Telescope. *Phys. Rev. Lett.*, 107:241302, 2011.
- [41] A. Albert et al. Searching for Dark Matter Annihilation in Recently Discovered Milky Way Satellites with Fermi-LAT. *Astrophys. J.*, 834(2):110, 2017.
- [42] G. Abbiendi et al. Search for Charged Higgs bosons: Combined Results Using LEP Data. *Eur. Phys. J. C*, 73:2463, 2013.
- [43] <https://atlas.web.cern.ch/Atlas/GROUPS/PHYSICS/CombinedSummaryPlots/HDBS/>.
- [44] <https://twiki.cern.ch/twiki/bin/view/CMSPublic/Summary2HMSRun2>.
- [45] A combination of measurements of Higgs boson production and decay using up to  $139 \text{ fb}^{-1}$  of proton–proton collision data at  $\sqrt{s} = 13$  TeV collected with the ATLAS experiment. Technical Report ATLAS-CONF-2020-027, CERN, Geneva, Aug 2020.
- [46] Otto Eberhardt. Current status of Two-Higgs-Doublet models with a softly broken  $\mathbb{Z}_2$  symmetry. *PoS, ICHEP2018:457*, 2019.
- [47] A. Arbey, F. Mahmoudi, O. Stal, and T. Stefaniak. Status of the Charged Higgs Boson in Two Higgs Doublet Models. *Eur. Phys. J. C*, 78(3):182, 2018.
- [48] G. Belanger, F. Boudjema, A. Pukhov, A. Semenov, and et al. The user’s manual, version 5.2, [http://lappth.cnrs.fr/micromegas/v5.2/manual\\_5.2.pdf](http://lappth.cnrs.fr/micromegas/v5.2/manual_5.2.pdf).
- [49] Philip Bechtle, Sven Heinemeyer, Tobias Klingl, Tim Stefaniak, Georg Weiglein, and Jonas Wittbrodt. HiggsSignals-2: Probing new physics with precision Higgs measurements in the LHC 13 TeV era. *Eur. Phys. J. C*, 81(2):145, 2021.
- [50] Werner Porod. SPheno, a program for calculating supersymmetric spectra, SUSY particle decays and SUSY particle production at  $e^+ e^-$  colliders. *Comput. Phys. Commun.*, 153:275–315, 2003.
- [51] Devin G. E. Walker. Dark Matter Stabilization Symmetries from Spontaneous Symmetry Breaking. 7 2009.
- [52] Brian Batell. Dark Discrete Gauge Symmetries. *Phys. Rev. D*, 83:035006, 2011.
- [53] Christian Gross, Oleg Lebedev, and Takashi Toma. Cancellation Mechanism for Dark-Matter–Nucleon Interaction. *Phys. Rev. Lett.*, 119(19):191801, 2017.
- [54] Chengfeng Cai, Yu-Pan Zeng, and Hong-Hao Zhang. Cancellation mechanism of dark matter direct detection in Higgs-portal and vector-portal models. 9 2021.
- [55] Florian Staub. SARAH 4 : A tool for (not only SUSY)

- model builders. *Comput. Phys. Commun.*, 185:1773–1790, 2014.
- [56] Giorgio Arcadi, Giorgio Busoni, Thomas Hugle, and Valentin Titus Tenorth. Comparing 2HDM + Scalar and Pseudoscalar Simplified Models at LHC. *JHEP*, 06:098, 2020.
  - [57] Philip Bechtle, Daniel Dercks, Sven Heinemeyer, Tobias Klingl, Tim Stefaniak, Georg Weiglein, and Jonas Witbrodt. HiggsBounds-5: Testing Higgs Sectors in the LHC 13 TeV Era. 6 2020.
  - [58] Philip Bechtle, Sven Heinemeyer, Oscar Stål, Tim Stefaniak, and Georg Weiglein. *HiggsSignals*: Confronting arbitrary Higgs sectors with measurements at the Tevatron and the LHC. *Eur. Phys. J. C*, 74(2):2711, 2014.
  - [59] Johan Alwall, Michel Herquet, Fabio Maltoni, Olivier Mattelaer, and Tim Stelzer. MadGraph 5 : Going Beyond. *JHEP*, 06:128, 2011.
  - [60] J. Alwall, R. Frederix, S. Frixione, V. Hirschi, F. Maltoni, O. Mattelaer, H. S. Shao, T. Stelzer, P. Torrielli, and M. Zaro. The automated computation of tree-level and next-to-leading order differential cross sections, and their matching to parton shower simulations. *JHEP*, 07:079, 2014.
  - [61] Pythia, <http://home.thep.lu.se/~torbjorn/pythia81html/Welcome.html>.
  - [62] J. de Favereau, C. Delaere, P. Demin, A. Giammanco, V. Lemaître, A. Mertens, and M. Selvaggi. DELPHES 3, A modular framework for fast simulation of a generic collider experiment. *JHEP*, 02:057, 2014.
  - [63] Michele Selvaggi. DELPHES 3: A modular framework for fast-simulation of generic collider experiments. *J. Phys. Conf. Ser.*, 523:012033, 2014.
  - [64] Alexandre Mertens. New features in Delphes 3. *J. Phys. Conf. Ser.*, 608(1):012045, 2015.
  - [65] The International Linear Collider Technical Design Report - Volume 3.II: Accelerator Baseline Design. 6 2013.
  - [66] B. Dumont, B. Fuks, S. Kraml, S. Bein, G. Chalons, E. Conte, S. Kulkarni, D. Sengupta, and C. Wymant. Toward a public analysis database for LHC new physics searches using MADANALYSIS 5. *Eur. Phys. J. C*, 75(2):56, 2015.
  - [67] Eric Conte, Béranger Dumont, Benjamin Fuks, and Chris Wymant. Designing and recasting LHC analyses with MadAnalysis 5. *Eur. Phys. J. C*, 74(10):3103, 2014.
  - [68] Eric Conte and Benjamin Fuks. Confronting new physics theories to LHC data with MADANALYSIS 5. *Int. J. Mod. Phys. A*, 33(28):1830027, 2018.
  - [69] Jack Y. Araz, Mariana Frank, and Benjamin Fuks. Reinterpreting the results of the LHC with MadAnalysis 5: uncertainties and higher-luminosity estimates. *Eur. Phys. J. C*, 80(6):531, 2020.
  - [70] Jack Y. Araz, Benjamin Fuks, and Georgios Polykratis. Simplified fast detector simulation in MADANALYSIS 5. *Eur. Phys. J. C*, 81(4):329, 2021.
  - [71] Addendum to the report on the physics at the HL-LHC, and perspectives for the HE-LHC: Collection of notes from ATLAS and CMS. *CERN Yellow Rep. Monogr.*, 7:Addendum, 2019.
  - [72] Amit Adhikary, Shankha Banerjee, Rahool Kumar Barman, and Biplob Bhattacharjee. Resonant heavy Higgs searches at the HL-LHC. *JHEP*, 09:068, 2019.
  - [73] H. Bahl, P. Bechtle, S. Heinemeyer, S. Liebler, T. Stefaniak, and G. Weiglein. HL-LHC and ILC sensitivities in the hunt for heavy Higgs bosons. *Eur. Phys. J. C*, 80(10):916, 2020.
  - [74] Georges Aad et al. Search for new phenomena in events with an energetic jet and missing transverse momentum in  $pp$  collisions at  $\sqrt{s}=13$  TeV with the ATLAS detector. *Phys. Rev. D*, 103(11):112006, 2021.
  - [75] Search for invisible Higgs boson decays with vector boson fusion signatures with the ATLAS detector using an integrated luminosity of 139 fb<sup>-1</sup>. Technical report, CERN, Geneva, Apr 2020. All figures including auxiliary figures are available at <https://atlas.web.cern.ch/Atlas/GROUPS/PHYSICS/CONFNOTES/ATLAS-CONF-2020-008>.
  - [76] Ties Behnke, James E. Brau, Brian Foster, Juan Fuster, Mike Harrison, James McEwan Paterson, Michael Peskin, Marcel Stanitzki, Nicholas Walker, and Hitoshi Yamamoto. The International Linear Collider Technical Design Report - Volume 1: Executive Summary. 2013. See also <http://www.linearcollider.org/ILC/TDR>. The full list of contributing institutes is inside the Report.
  - [77] G. Moortgat-Pick et al. The Role of polarized positrons and electrons in revealing fundamental interactions at the linear collider. *Phys. Rept.*, 460:131–243, 2008.
  - [78] T. K. Charles et al. The Compact Linear Collider (CLIC) - 2018 Summary Report. 2/2018, 12 2018.
  - [79] Philipp Gerhard Roloff and Aidan Robson. Updated CLIC luminosity staging baseline and Higgs coupling prospects. Technical report, CERN, Geneva, Oct 2018. 9 pages, 6 figures.
  - [80] A. Blondel, J. Gluza, S. Jadach, P. Janot, and T. Riekmann, editors. *Theory for the FCC-ee: Report on the 11th FCC-ee Workshop Theory and Experiments*, volume 3/2020 of *CERN Yellow Reports: Monographs*, Geneva, 5 2019. CERN.
  - [81] Mingyi Dong et al. CEPC Conceptual Design Report: Volume 2 - Physics & Detector. 11 2018.
  - [82] Halina Abramowicz et al. The International Linear Collider Technical Design Report - Volume 4: Detectors. 6 2013.
  - [83] Glen Cowan, Kyle Cranmer, Eilam Gross, and Ofer Vitells. Asymptotic formulae for likelihood-based tests of new physics. *Eur. Phys. J. C*, 71:1554, 2011. [Erratum: *Eur.Phys.J.C* 73, 2501 (2013)].
  - [84] <https://pdg.lbl.gov/2019/reviews/rpp2018-rev-statistics.pdf>.
  - [85] Gerard Jungman, Marc Kamionkowski, and Kim Griest. Supersymmetric dark matter. *Phys. Rept.*, 267:195–373, 1996.